Available online at www.sciencedirect.com

SCIENCE DIRECT®

Journal of Marine Systems 51 (2004) 95–122

JOURNAL OF MARINE SYSTEMS

www.elsevier.com/locate/jmarsys

HF radar observations in the northern Adriatic: surface current field in front of the Venetian Lagoon

V. Kovačević[a,*], M. Gačić[a], I. Mancero Mosquera[b,1], A. Mazzoldi[c], S. Marinetti[d]

[a]*Istituto Nazionale di Oceanografia e di Geofisica Sperimentale (OGS), Borgo Grotta Gigante 42/c, 34010 Sgonico, Trieste, Italy*
[b]*Escuela Superior Politécnica del Litoral, Guayaquil, Ecuador*
[c]*C.N.R.-Istituto di Scienze Marine, Sezione di Ricerca di Venezia, Italy*
[d]*C.N.R.-Istituto per le Tecnologie della Costruzione-Sezione di Padova, Italy*

Received 15 December 2002; accepted 19 May 2004
Available online 19 August 2004

Abstract

Two HF radar stations looking seaward were installed along the littoral of the Venetian Lagoon (Northern Adriatic). They operated continuously for 1 year (November 2001–October 2002). The surface current data are obtained at a spatial resolution of about 750 m and are available every hour in a zone whose depths slope gently from the coast down to 20 m. The total area covered is about 120 km^2 reaching cca 15 km offshore. These observations give evidence of the different temporal and spatial scales that characterize the current field. Unlike for the flow in inlets of the Venetian Lagoon, the tidal forcing accounts for only up to 20% of the total variability. The tidal influence from the inlets is felt to about 4–5 km away. Low-frequency signal, associated prevalently to meteorological forcing (through the action of winds and atmospheric pressure) at synoptic time scales, is superimposed on a mean southward flow of 10 cm/s. Formation of small-scale eddies (diameter of about 5 km) to the north and to the south of the Malamocco inlet is observed only during the periods of calm. During strong northeasterly bora and southeasterly sirocco winds, an increase of the along-shore southward current due to geostrophic adjustment is observed in a coastal band. A particularly strong bora event in December 2001 generated an almost uniform flow reaching 30–50 cm/s in the whole investigated area. During sirocco in June 2002, a current reversal toward north and a triggering of inertial motions were observed. Yearlong measurements give an insight into a seasonal variability through a sequence of mean monthly current maps. In November and December, the intensity was the highest (up to 18 cm/s), and the flow structure was almost uniform, with a weak shear in the offshore direction. The weakest mean flow was observed in May 2002, characterized however with a nonuniform distribution over the study zone and suggestions of anticyclonic eddies north and south of the Malamocco inlet. On the other hand, possibly due to the highly variable wind,

* Corresponding author. Tel.: +39 40 2140 292; fax: +39 40 2140 266.
E-mail address: vkovacevic@ogs.trieste.it (V. Kovačević).
[1] Presently at OGS, Trieste, Italy.

0924-7963/$ - see front matter © 2004 Elsevier B.V. All rights reserved.
doi:10.1016/j.jmarsys.2004.05.026

the eddy kinetic energy in May, associated with both small-scale variability near the shore and inertial oscillations offshore, was maximum for the investigated period.
© 2004 Elsevier B.V. All rights reserved.

Keywords: Surface currents; HF radar; Tides; Residual currents; Winds; Adriatic Sea; Venetian Lagoon

1. Introduction

The Venetian Lagoon and its surroundings have been a focus of scientific and research interest over the past decades. It is one of the coastal regions of the Adriatic Sea (Fig. 1), which concentrates human settlements, industry, tourism, and rich historic heritage. The need for preservation, management, and sustainable development of the lagoon has resulted in series of interdisciplinary studies. One of the latest intensive programmes of research has been set up by Consortium for Coordination of Research Activities concerning the Venice Lagoon System (CORILA) for the period 2000–2004. In the framework of this programme, monitoring of the surface currents began in 2001. The aim of this activity has been to collect data on the surface circulation in front of the Venetian Lagoon, continuously, for a long-term period. The area monitored covers about 120 km^2 with a spatial resolution of 750 m. The sampling was designed to complement other monitoring activities, like measuring the water flow in the lagoon inlets, which all together should provide answers to the questions regarding interaction between the lagoon and the open sea.

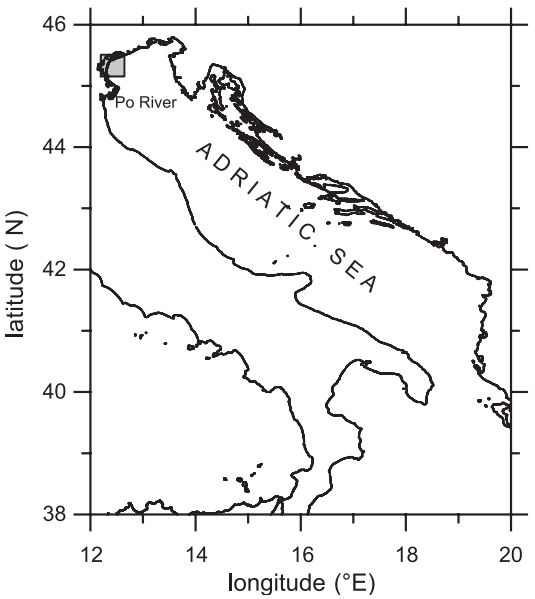

Fig. 1. Rectangular zone depicts the study zone offshore of the Venetian Lagoon in the northern part of the Adriatic Sea.

The scope of the present paper is to describe principal characteristics of the circulation and its variability both in time and space. The main properties of the tidal signal will be discussed, i.e., spatial pattern of the most significant semidiurnal (M2) and diurnal (K1) tidal constituents will be mapped. The response of the subtidal current field to strong wind conditions during bora and sirocco events will be examined. Finally, the monthly mean flow characteristics and variability will be discussed. The possible interaction with the flow within the inlets will be addressed as well. We are aware of the main drawback of our approach, which deliberately excludes some other factors that can influence the flow pattern in this coastal region, such as stratification and bathymetry. In this paper, we do not discuss directly the possible influence of the stratification nor some episodic events, like high freshwater discharge from the rivers surrounding the study area, among which the Po River to the south is the greatest source of fresh water (Raicich, 1996). We assume at the moment that the bathymetry effect is small, mainly due to the smoothly increasing bottom depth, due to the isobaths trending parallel to the coast, and due to the fact that the major portion of the study area lies between the 10 and 20 m isobaths. The bathymetry and the coastal morphology may affect the small-scale circulation, like the eddy formation on the seaward wake of the lagoon littoral as will be just mentioned in our analysis. An analysis of stratification, bottom topography, and coastal morphology influences deserves a detailed approach, which is beyond the scope of the present paper.

The manuscript is organized as follows: Section 2 overviews the basic principles of the radar technique for measuring surface currents, data treatment, and statistical methods used for the data analysis; Section

3 outlines the results of the analysis; Section 4 brings up the conclusions.

2. Data and methods

2.1. HF radar installations

The shore-based, high-frequency (HF) radar systems installed in the study area are SeaSonde units produced by Codar Ocean Sensors (COS), which consist of compact transmitting and receiving antennas. The systems are set up with a 25 MHz operating frequency. Each radar station consists of one transmitting and one receiving antenna and is capable of determining radial currents to and from it out to distances as far as about 15 km offshore. The Bragg scattering of the electromagnetic radiation over a rough sea is a basic physical mechanism on which the technology of the HF radars is founded (Crombie, 1955). This mechanism is based on a property of an electromagnetic wave at a given frequency to scatter on the ocean waves of exactly the half wavelength, which for our radars means that a 12-m wave (corresponding to a 25 MHz transmitting frequency) is backscattered from the 6-m surface waves. The application of this property has evolved in the past three decades, and the HF radars, especially the shore-based, and to a lesser extent, those ship-borne, have become a powerful complementary technique in coastal ocean studies, as reported in some of the many bibliographic sources (Barrick et al., 1974, 1977; Gurgel et al., 1999; Paduan and Rosenfeld, 1996; Paduan and Graber, 1997).

The software of the system produces complex cross-spectra of the received echo for each station every 2.5 min. Every 10 min, these data are averaged over a time interval of 15 min and converted into 10-min radials. Those are used for determining the hourly radial velocities at 5° angular resolution, providing bearing, range, and speed. The radial data from two or more stations are then combined to produce hourly maps of vector currents within a regular grid. The vector computations utilize radials within a 30–150° sector with respect to the baseline that connects two locations. Beyond that sector, radial velocity uncertainties increase due to increased propagation loss and signal refraction effects (Lipa and Barrick, 1983). In addition, the intersection angles between the radials that are combined into total vectors should also be between 30° and 150° (Paduan and Graber, 1997) to resolve better the current vector. Typical nominal accuracy of total vectors is less than 7 cm/s in magnitude and less than 10 degrees in direction, as specified by the producer (COS, http://www.codaros.com/seasonde_specs.htm).

In this study, two radar stations, located at the Lido and Pelestrina islands and distant about 10 km from each other, operated continuously from November 2001 through October 2002. A third unit, situated on the Oceanographic Platform of the ISMAR–CNR, about 15 km offshore from the Malamocco inlet, was operating intermittently. Its data have not been taken into account in the present study. The two radar stations at the islands provided a long-term time series of hourly currents over the study zone depicted in Fig. 2, starting on 1 November, 2001, at 00:00 and ending on October 31, 2002, at 23:00 h. All dates and times in this paper refer to a Coordinated Universal Time (UTC).

The study area (Fig. 2) is situated in front of the Malamocco inlet, where the sea floor slopes gently from shallow coastal depths to about 20-m depth offshore. Grid points are about 750 m distant from each other. Thick dots are those for which radial vectors from the two antennas intersect at angles between 30° and 150°, as suggested by Paduan and Graber (1997). Reliable current vectors can be determined for the central open sea area in front of the islands of Lido and Pelestrina, including the zone in the vicinity of the Malamocco inlet. In that area, the data return over the yearlong measurement interval (calculated as the ratio between the number of hours with data available and total number of hours, 8760) was maximum, as shown in Fig. 2. Unfortunately, the spatial resolution is not high enough to map the currents inside the inlets, which would be interesting for the comparison with the ongoing current measurements within the channels using self-contained moored ADCPs (see paper by Gačić et al., 2004).

In our analysis, we have included all the grid points with the data return greater than 60%. As stated by Paduan and Rosenfeld (1996), the data returns may provide a crude measure of the reliability of the data set, so they considered their 50% coverage contour as a lower limit for the data inclusion. In absence of some other more objective technique, like the one that is implemented in the latest version of the SeaSonde

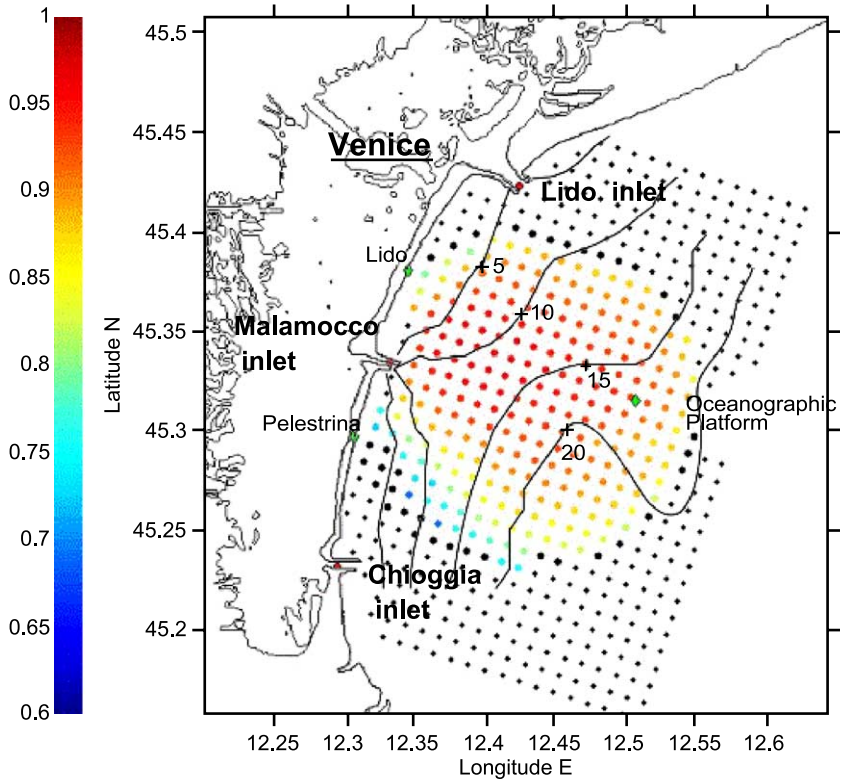

Fig. 2. Domain of HF radar measurements superimposed over an approximate bathymetric chart (depths are in metres). Diamonds show the location of the antennas at Lido, Pelestrina, and the Oceanographic Platform. Thin dots denote the grid due to the three antennas. Thick dots represent the grid due to the two antennas at the islands. Colour bar denotes data return over the 1-year time interval for the grid nodes used in the analysis. Wind data are available from the Oceanographic Platform.

software known as geometrical dilution of statistical accuracy (Don Barrick, personal communication), we rely upon the data return map, taking as a lower limit 60% of the data return. The goodness of our approach will be validated once a new data set has been collected, hopefully using three antennas, and analysed using the new software to provide parameters for the realistic determination of the geometric dilution of statistical accuracy. With the third station operating, the covered area will be twice as large and will include the vicinities of Lido and Chioggia inlets (Fig. 2).

2.2. Data treatment

Before the analyses were conducted, the hourly data, supplied as two current components (u-positive eastward, v-positive northward) were checked for spikes, i.e., anomalous values that appear occasionally induced by errors in target speed or location determinations. Environmental noise, radio interference, and relatively dense sea traffic in front of the lagoon are the most probable causes for such errors. The spikes were individuated in this way: the first differences were calculated from the original data set in order to achieve a second-order stationarity (mean and variance are more steady than in the original data set). To a certain extent, the differenced data, as evidenced from our analysis (not shown here), satisfy conditions of a normal distribution. Therefore, a threshold was determined at $\pm 2.58 \times$std (std being a standard deviation). Within these limits, 99% of the data is included. Hence, all those that fell outside this interval were investigated as possible error spikes. The necessary requirement was: if one value was suspected and fell at the 0.5% extreme end of the distribution and then the next value in time fell at the other 0.5% extreme end of the

distribution, the suspected value indicated a spike that was eliminated from the original data set. In such a way, single-hour anomalous values were removed. An additional check was performed in order to identify possible remaining spikes and eliminate them. For instance, 2-h spikes (two consecutive spikes) were identified by examining three succeeding values, the first of which was a suspected value lying at the 0.5% extreme end of the distribution and the third one was a suspected value lying at the other 0.5% extreme end of the distribution. In these situations, the indicated two anomalies in the original time series were eliminated. The 'cleaned' time series, called despiked hourly data, were the basis of all subsequent analyses.

2.3. Basic methods for time-series analysis

A power spectrum, obtained by a complex Fast Fourier Transform (FFT), is a tool that distributes the total variance over a range of frequencies. With a sampling interval of 1 h, the Nyquist frequency, i.e., the highest frequency that can be resolved, is 0.5 cph. Several locations were chosen in order to assess spectral variations between the near-shore and offshore regions. The application of the rotary spectrum analysis to the u and v current components enables a separation of the energy into clockwise or negative sense (indicated by negative frequencies) and counter clockwise or positive sense (indicated by positive frequencies) of the current vector rotation. The essential requirement for applying a classical FFT method is the continuity of the data record. Therefore, the time series of the current components were inspected for gaps, both initial and those created by spike eliminations. When the gap size was not larger than 6 h, it was linearly interpolated. A search for subsets long enough for applying the spectral analysis resulted in the choice of the three periods: the first one is representative for the autumn–winter season (AW), the second one for the spring (Sp), and the third one for the summer season (Su). Details about the three periods are reported in Table 1. Such a choice enables us to compare the power spectrum for different times of the year. Each data set was divided into 256-size 50% overlapping segments. On each segment, the FFT was preformed. The Hamming window, aimed at reducing the side lobes of the spectral output from FFT routines, was applied, yielding to the frequency resolution of 0.01414 cph.

Harmonic analysis, based on Foreman (1978), was performed using a number of routines for MatLab programming. For this purpose, a yearlong hourly time series from all the available grid nodes, with spikes eliminated but not interpolated, were analysed. This was done in order to determine the tidal characteristics (amplitudes and phases) of the most significant constituents as well as their spatial patterns.

2.4. Eddy kinetic energy calculation for nontidal currents

The nontidal currents were calculated by subtracting the tidal constituents from the despiked hourly data. All tidal constituents, for which the signal-to-noise ratio exceeded 1, were removed. On the basis of these nontidal hourly data, mean yearly and monthly current maps were plotted. The mean Eddy Kinetic Energy per unit mass, [EKE], expressed as

$$[\mathrm{EKE}] = \sum_{i=1}^{N} \left[(u_\mathrm{i} - u_\mathrm{a})^2 + (v_\mathrm{i} - v_\mathrm{a})^2 \right] / 2N$$

was calculated for all grid nodes, where u_i and v_i represent eastward and northward hourly components, N is the total number of hours in a monthly time interval, and u_a and v_a are the corresponding monthly mean values.

Table 1
Selection of the data for spectral analysis of currents and wind for the three time intervals

Season	Parameter	Location	Time interval	Total duration
AW period:	currents	A, B, C	2001/11/01 00:00–2002/01/05 19:00	1580 h
Autumn–Winter	wind	Oceanographic platform	2001/11/01 00:00–2001/12/09 22:00	935 h
Sp period: Spring	currents	A, B, C	2002/04/18 15:00–2002/06/17 07:00	1433 h
	wind	Oceanographic platform	2002/04/18 15:00–2002/05/28 10:00	956 h
Su period: Summer	currents	A, B, C	2002/06/27 09:00–2002/09/05 05:00	1677 h
	wind	Oceanographic platform	2002/06/27 09:00–2002/09/05 05:00	1677 h

2.5. Subtidal currents

The nontidal currents still contain some high-frequency fluctuations, such as inertial oscillations. In order to relate the currents to some particular wind conditions, those high-frequency motions were eliminated by low-pass filtering. Prior to that, the missing data in the nontidal time series were linearly interpolated for the gaps that did not exceed 6 h. The whole time series was thus composed of a number of continuous segments. A digital symmetric low pass filter (Hamming window with 25 weights) was applied to those segments whose lengths were at least a threefold filter length. Subtidal currents were then used for mapping the hourly flow field in conjunction with some extreme wind conditions in order to illustrate the wind-forced low-frequency response.

2.6. Wind data

Wind measurements from the C.N.R. Oceanographic Platform 'Acqua Alta', sampled every 5 min, were taken as representative of the local open sea wind conditions. Mean hourly values of wind vectors were calculated as an average from all the data available within a time interval +/−30 min around the cardinal hour. Spectral analysis of the wind data was performed as for the current data. Gaps in the wind time series, however, limited the record length of the subsets. For details, see Table 1.

3. Analysis of results

3.1. Spatial and temporal current variability from rotary power spectrum

In this section, rotary power spectra of hourly current data are presented for three seasons at three different distances from the Malamocco inlet.

Fig. 3a characterizes the AW season. The low-frequency oscillations (<0.02 cph; i.e., with periods >50 h), diurnal (≈0.04 cph) and semidiurnal (≈0.08 cph) tidal constituents account for most of the variance. The low-frequency signal prevails over the tidal one at all three locations. In general, variability seems to be more intense near the coast, as shown for the grid node A. A diurnal peak for both the positive and negative sense of rotation is much more evident near the coast than offshore. During the AW period near the coast, the diurnal and semidiurnal bands are distributed almost symmetrically around the zero frequency, showing that the motion is almost rectilinear at these frequencies. Moving offshore, the semidiurnal band is much more evident for the positive sense of rotation, suggesting prevalence of rotational motions.

Fig. 3b reports the rotary power spectrum for the Sp season, during which low-frequency variability is reduced with respect to the high-frequency oscillations. Moreover, the inertial currents, with a period of oscillation of about 17 h (~0.06 cph) in the negative sense of rotation, become evident and increase seaward. During the Su season, the inertial signal is even more pronounced (Fig. 3c) and increases slightly in the offshore direction. Both in Sp and Su, the diurnal peak for the negative sense of rotation becomes dominant. The asymmetry increases from winter to summer, especially due to the enhanced diurnal signal and inertial oscillations at negative frequencies (clockwise rotation), which increase in the offshore direction. This indicates a prevalence of the rotational motion over the rectilinear ones, particularly in the open sea area.

3.2. Tidal motions

Harmonic analysis of the hourly time series at selected points provides more details about the properties of tidal ellipses of single constituents, which are reported in Table 2 at selected grid nodes. Seven tidal constituents typically used in a tidal analysis of the sea

Fig. 3. Two-sided rotary spectrum of hourly currents at three locations indicated in the inserted map: near the Malamocco inlet (A), in the central region (B), and close to the Oceanographic Platform (C). Three different time intervals were examined: AW (a), Sp (b), and Su (c). For details, see Table 1. Vertical and horizontal error bars denote the 95% confidence level and a frequency resolution, respectively. Negative frequencies refer to the clockwise (anticyclonic) motions, while positive frequencies refer to the counterclockwise (cyclonic) motions. The area below the curve corresponds to the total variance. Vertical dashed lines indicate the following periodical motions (from left to right): 11-h seiches, K2, S2, M2, N2, inertial (16.97 h), 22-h seiches, K1, P1, O1 (for negative frequencies), and O1, P1, K1, 22-h seiche, N2, M2, S2, K2, 11-h seiches (for positive frequencies).

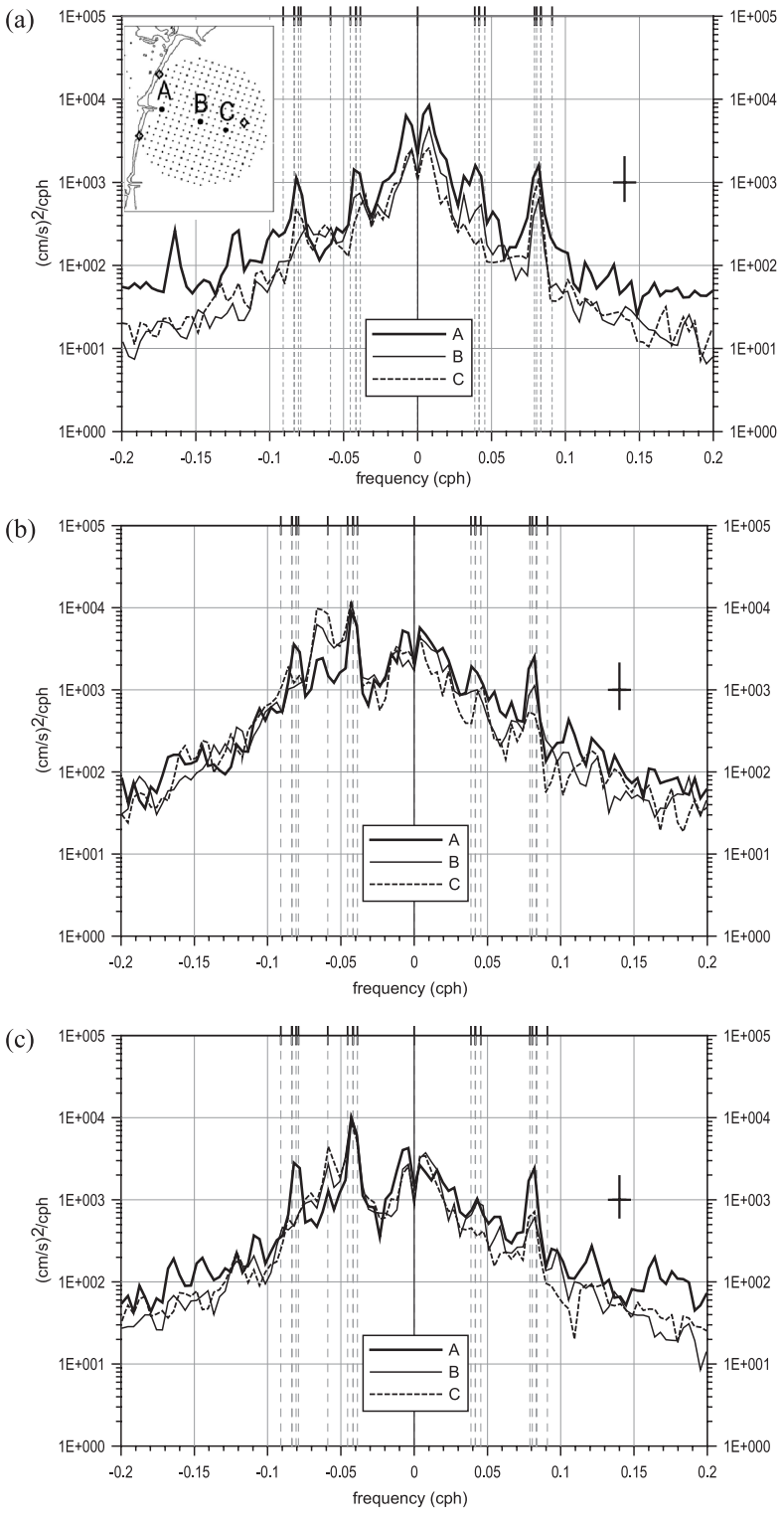
(a)
(b)
(c)
A
B
C
(cm/s)2/cph
frequency (cph)
1E+005
1E+004
1E+003
1E+002
1E+001
1E+000
-0.2
-0.15
-0.1
-0.05
0
0.05
0.1
0.15
0.2

Table 2
Tidal ellipse parameters of typical seven tidal constituents at selected grid nodes A, B, and C (Fig. 3) in front of Malamocco inlet

Tidal constituent	Period (h)	Semi-major (cm/s)	Error (cm/s)	Semi-minor (cm/s)	Error (cm/s)	Direction (degrees)	Error (degrees)	Phase (degrees)	Error (degrees)	Eccentricity	Explained variance (%)
Location A											
M2	12.42	6.3	0.7	−0.1	0.7	0	6	73	6	−0.02	5.4
S2	12.00	2.9	0.7	0.3	0.6	11	14	84	16	0.10	1.1
K2	11.97	0.7	0.6	0.1	0.5	−3	49	103	60	0.14	0.1
N2	12.66	1.0	0.7	0.0	0.6	9	40	81	41	0.00	0.1
K1	23.93	4.9	1.1	−1.1	0.9	−3	9	194	12	−0.22	3.4
P1	24.07	2.3	1.0	−1.0	0.9	−26	35	185	34	−0.43	0.8
O1	25.82	2.4	1.1	0.1	0.7	6	21	222	27	0.04	0.7
Z_0		7.3									Total: 11.6
Location B											
M2	12.42	2.1	0.7	0.7	0.6	1	20	62	24	0.33	0.9
S2	12.00	1.0	0.6	0.8	0.6	−31	98	37	97	0.80	0.3
K2	11.97	0.3	0.5	0.1	0.4	−79	145	27	143	0.33	0.0
N2	12.66	0.4	0.6	−0.2	0.5	−17	77	78	130	−0.50	0.0
K1	23.93	3.8	1.1	−1.4	1.1	−29	20	191	20	−0.37	2.8
P1	24.07	2.6	2.6	−1.7	0.9	−46	57	188	55	−0.65	1.7
O1	25.82	1.4	0.9	−0.2	1.0	−25	43	219	48	−0.14	0.4
Z_0		9.4									Total: 6.1
Location C											
M2	12.42	2.7	0.7	1.1	0.7	−40	18	345	20	0.41	1.6
S2	12.00	2.0	0.7	0.4	0.7	−50	21	343	22	0.20	0.8
K2	11.97	0.5	0.5	0.0	0.6	−22	55	324	53	0.00	0.1
N2	12.66	0.4	0.5	0.0	0.5	−48	87	321	76	0.00	0.0
K1	23.93	3.0	0.9	−1.7	1.0	−27	38	173	36	−0.57	2.2
P1	24.07	2.1	1.0	−1.6	0.9	88	73	38	75	−0.76	1.3
O1	25.82	0.7	1.0	−0.4	0.8	−30	112	232	110	−0.57	0.1
Z_0		8.1									Total: 6.1

Amplitudes for semimajor and semiminor axes, direction and phase, with their respective errors are reported. Direction is positive if counterclockwise from the east and negative if clockwise from the east. Eccentricity is defined as the ratio between the minor and major axis amplitude, while the sense of rotation is denoted by the signs: + is for clockwise , and − is for anticlockwise rotation. Z_0 is the mean current velocity over the time interval considered after the removal of all the tidal constituents, whose signal to noise ratio (amplitude^2/error^2) is >1. Period considered: November 1, 2001, 00:00–October 31, 2002, 23:00.

level along the coast of the Adriatic Sea, M2, S2, K2, N2, O1, P1, and K1 are taken into consideration. The ellipse properties of the seven semidiurnal and diurnal motions show that the tidal currents are pretty small. At location A, about 1 km distant from the inlet, the most significant constituents from the two groups, namely, M2 and K1, reach 6.3 and 4.9 cm/s in amplitude, respectively. The tidal currents are relatively rectilinear (eccentricity is around 0.10), showing how this region is still influenced by the tidally driven flow inside the inlet of Malamocco. Moving further offshore, the amplitudes are decreasing. Hence, the errors of the direction are increasing. Even the highest tidal amplitudes are lower than the long-term mean current velocity, which varies between 7.3–9.3 cm/s for the three selected locations. The percentage of the total variance on a yearly time scale that can be attributed to the tidal forcing ranges from about 6% offshore (location C) to about 12% near-shore (location A), meaning that a low-frequency flow in general and inertial motion during spring and summer, accounts for the bulk of the variance.

The seven analysed constituents, which adequately describe the sea surface tidal elevations along the Adriatic coast (see a review by Cushman-Roisin et al., 2001), do not account for the major portion of the total

variance in the current field. If all constituents with a signal-to-noise ratio >1 are taken into account, the percentage of the total variance explained reaches 18% within 1 km distance from the inlet (location A) and about 10% further away (locations B and C). In Table 3, the seven constituents ordered with respect to their contribution to the total variance are reported. Among them, M2 remains as a principal tidal constituent near the inlets, while further offshore, the importance of semidiurnal motion diminishes and diurnal K1 prevails. Moreover, long-term constituents such as SSA (period of 182.588 days), MM (27.554 days), MSM (31.812 days), and MF (13.66 days) become more important than some diurnal and semidiurnal constituents. They, apart of the astronomical tidal signal, may contain some of the long-term variabilities of different origin (due to a meteorological or seasonal forcing).

Spatial distribution of the properties of the two major constituents is presented in Figs. 4–6. In Fig. 4, the tidal ellipses of both M2 and K1 in the vicinity of the inlet are strongly polarized under the influence of the tidal flow in the inlet (Gačić et al., 2004). Better insight into the amplitude distribution is obtained from Fig. 5. The amplitudes decrease moving offshore from the inlet. The maximum values of about 7 and 4 cm/s for M2 and K1, respectively, close to the inlet reduce to about 2–3 cm/s in the open sea. Phases in Fig. 6 show how the tidal signal propagates radially from the lagoon inlet. This is evident especially for the M2 constituent, for which the influence from the inlet is felt up to 6 km away. Overall, it is clear from these results how the signal associated with the tidal plume from the Malamocco inlet vanishes moving offshore. It would be of interest to compare these findings with those of a

Table 3
Same as Table 2, except for the seven constituents, which account for the major portion of the total variance

Tidal constituent	Period (h)	Semimajor (cm/s)	Error (cm/s)	Semiminor (cm/s)	Error (cm/s)	Direction (degrees)	Error (degrees)	Phase (degrees)	Error (degrees)	Eccentricity	Explained variance (%)
Location A											
M2	12.42	6.3	0.7	−0.1	0.7	0	6	73	6	−0.02	5.4
K1	23.93	4.9	1.1	−1.1	0.9	−3	9	194	12	−0.22	3.4
SSA	4382.12	3.4	2.8	−0.4	2.6	36	59	239	56	−0.12	1.5
MM	661.29	2.8	2.6	−0.8	2.3	33	64	299	79	−0.29	1.1
S2	12.00	2.9	0.7	0.3	0.6	11	14	84	16	0.10	1.1
P1	24.07	2.3	1.0	−1.0	0.9	−26	35	185	34	−0.43	0.8
O1	25.82	2.4	1.1	0.1	0.7	6	21	222	27	0.04	0.7
											Total: 14
Location B											
K1	23.93	3.8	1.1	−1.4	1.1	−29	20	191	20	−0.37	2.8
P1	24.07	2.6	2.6	−1.7	0.9	−46	57	188	55	−0.65	1.7
MM	661.29	2.2	2.3	−0.7	2.0	69	65	290	104	−0.32	1.0
M2	12.42	2.1	0.7	0.7	0.6	1	20	62	24	0.33	0.9
MSM	763.48	1.6	2.5	−0.3	2.0	76	60	78	127	−0.19	0.5
SSA	4382.12	1.4	2.6	0.7	2.1	−75	64	79	126	0.50	0.4
O1	25.82	1.4	0.9	−0.2	1.0	−25	43	219	48	−0.14	0.4
											Total: 7.7
Location C											
K1	23.93	3.0	0.9	−1.7	1.0	−27	38	173	36	−0.57	2.2
M2	12.42	2.7	0.7	1.1	0.7	−40	18	345	20	0.41	1.6
P1	24.07	2.1	1.0	−1.6	0.9	88	73	38	75	−0.76	1.3
S2	12.00	2.0	0.7	0.4	0.7	−50	21	343	22	0.20	0.8
MSM	763.48	1.5	2.0	−0.7	2.1	−58	110	207	109	−0.47	0.5
MM	661.29	1.6	1.9	−0.4	2.0	53	95	288	97	−0.25	0.5
MF	327.86	1.3	1.7	0.4	1.9	76	104	305	114	0.31	0.4
											Total: 7.3

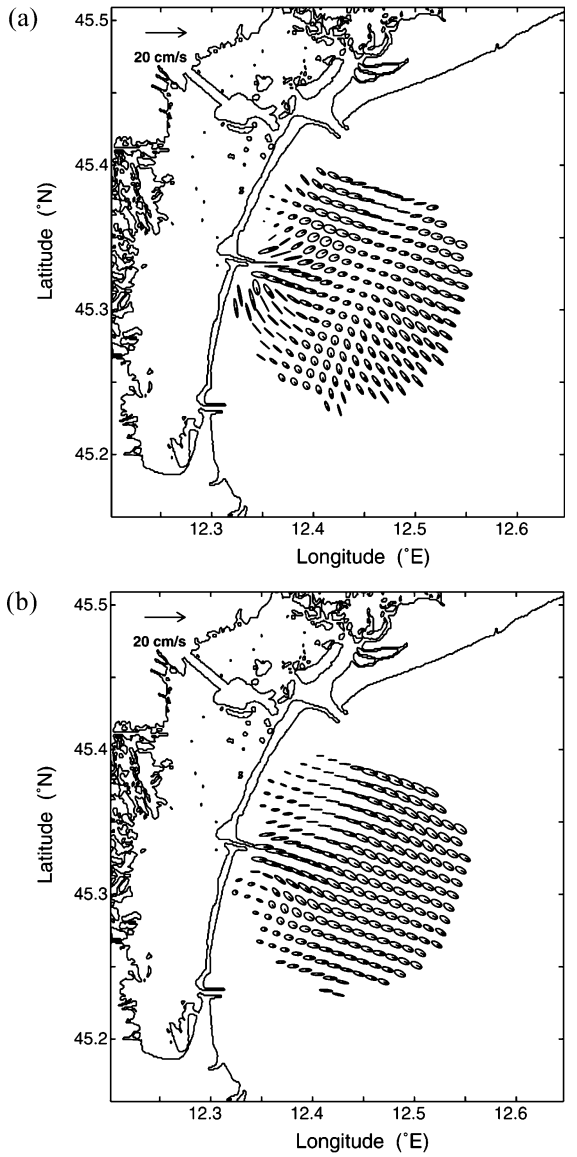

Fig. 4. Tidal ellipses of the M2 (a) and K1 (b) constituents.

numerical tidal model applied with sufficient resolution to the Venetian Lagoon and the adjacent open sea area. To date, studies of the tidal motions in the Adriatic Sea have involved mostly large-scale dynamics and just a few coastal zones (see Cushman-Roisin et al., 2001 for a review). In general, experimental studies in the Adriatic have been conducted mostly at the open sea (e.g., Ursella and Gačić, 2001).

3.3. Nontidal currents and wind

The previous analyses have shown that tidal motions explain a relatively small portion of the total surface current variability. Spectral analyses were performed on the nontidal current time series as well, which may contain variability due to the influence of local and remote winds, horizontal pressure gradient,

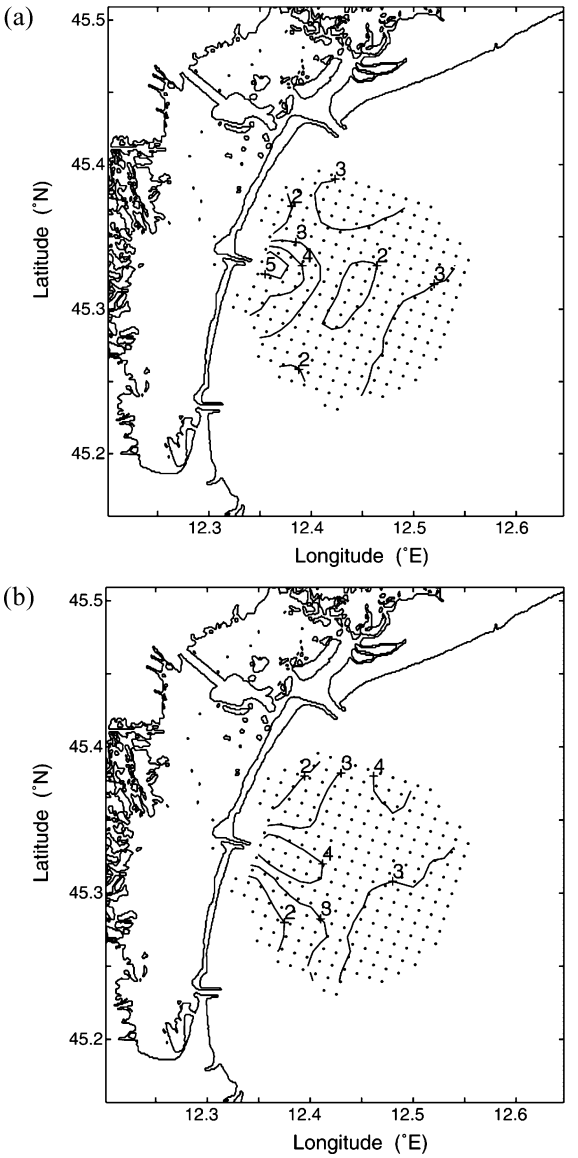

Fig. 5. Contour lines of amplitudes in cm/s for the M2 (a) and K1 (b), referring to a semimajor axis of the tidal ellipse.

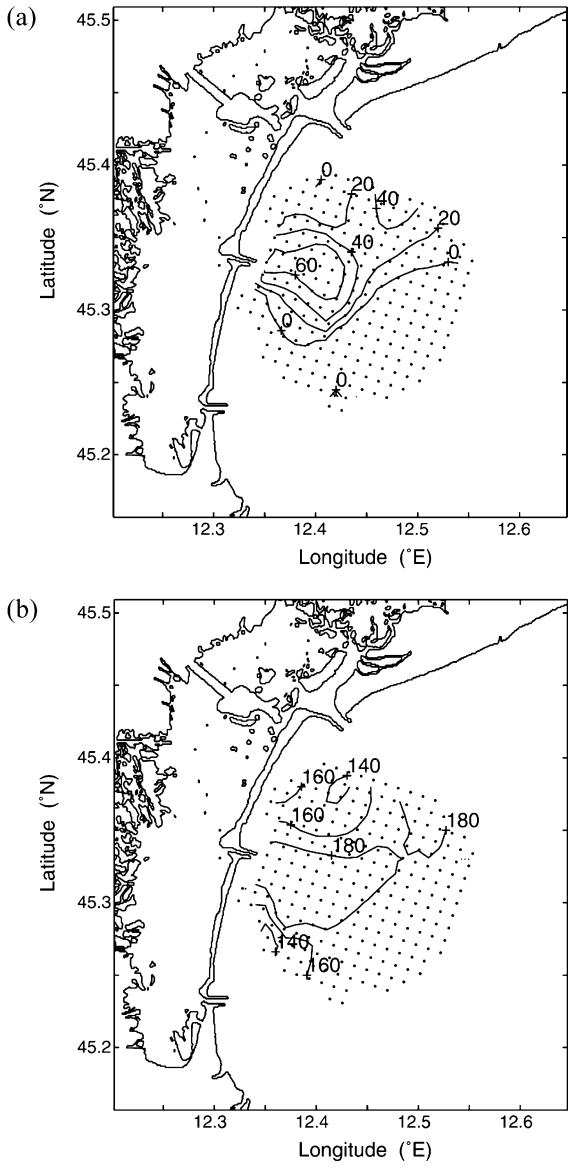

Fig. 6. Contour lines of the phases in degrees for the M2 (a) and K1 (b) tidal constituents.

etc. Except for the possible influence of the sea breeze on the surface circulation during spring and summer seasons when diurnal wind variations are dominant, wind action is prominent only in stormy weather conditions. These conditions occur during the strong northeasterly bora wind and the southeasterly sirocco wind (for details, see Poulain and Raicich, 2001). Below, we illustrate the subtidal current field associated with two such wind episodes. In addition, current field evolution corresponding to variable winds during one week in May is also shown.

3.3.1. Seasonal similarities and differences: AW, Sp, and Su

It is evident that during AW (Fig. 7a), low-frequency signals prevail in the current field, while during Sp (Fig. 7b) and Su (Fig. 7c), the variance contained between the inertial and diurnal frequencies, particularly in the negative sense of rotation, dominates the low-frequency motions. The secondary peak in the clockwise portion of the spectrum may be attributed to the diurnal seiche because it is close to the diurnal band of the basin-wide principal Adriatic seiche mode, 21.4–22.4 h (Cushman-Roisin et al., 2001). Inertial signal increases offshore in absolute terms, as well as with respect to other variabilities. The occurrence of the inertial motions further offshore during warm season is a phenomenon that has been observed at several locations of the Adriatic shelf (Orlić, 1987; Krajcar and Orlić, 1995).

The rotary power spectra of the hourly wind data show seasonal variability, as evidenced in Fig. 8. The asymmetric form of the spectra with respect to zero frequency becomes more and more evident passing from AW to Sp and Su. During AW (Fig. 8a), dominant peaks are in the low-frequency band at synoptic time scales of the order of several days. In Sp (Fig. 8b), in addition to the low-frequency band, diurnal oscillations in the clockwise sense of rotation appear. These fluctuations increase during Su (Fig. 8c), prevailing over the low-frequency band. Such a peak during Sp and Su periods may be related to the sea breeze regime during the warm season (Orlić et al., 1988). This might also give a reasonable explanation for a general increase of the clockwise diurnal rotation of the nontidal surface currents evident in Fig. 7b and c because the sea breeze induces variability close to the frequency of the diurnal seiche.

3.3.2. Wind variability

It has already been shown that the wind conditions influence appreciably the currents in the Adriatic Sea (Orlić et al., 1992, 1994, Bergamasco and Gačić, 1996; Poulain and Raicich, 2001 for a review). In order to illustrate the local wind conditions over the

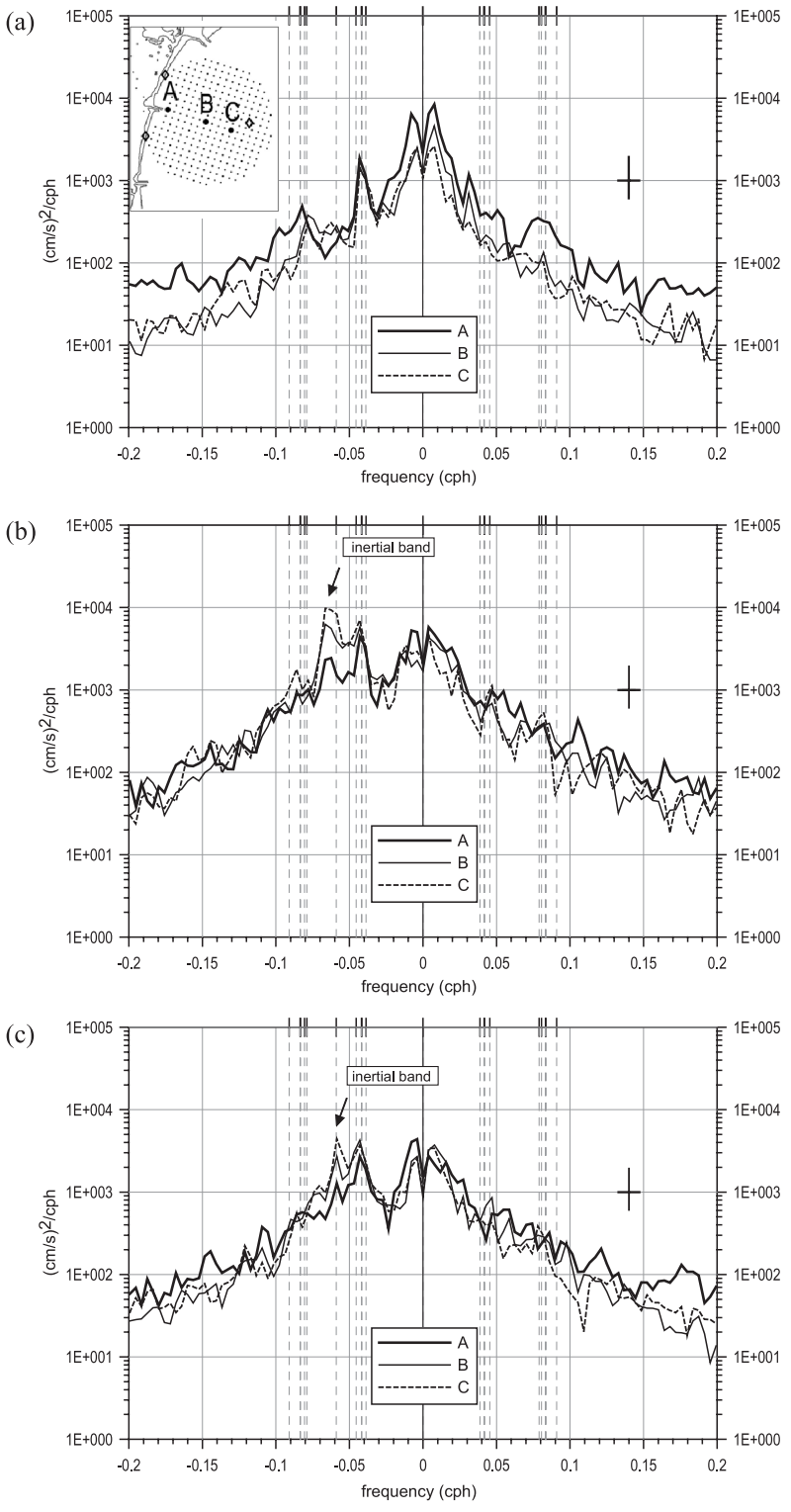

Fig. 7. The same as Fig. 3, except for the nontidal (detided) hourly currents.

study area in some particular periods, hourly mean wind vectors are plotted in Fig. 9. For that purpose, we have chosen four months: December 2001, January 2002, May 2002, and June 2002. Strong NE bora winds occurred in December. This is a relatively frequent event during the cold season, when local weather conditions are influenced by the passages of synoptic atmospheric perturbations, cyclones and anticyclones, which both may provoke strong northeasterly winds over the Northern Adriatic (for a review of the climate of the Adriatic Sea, see Cushman-Roisin et al., 2001). The maximum hourly speed of 23 m/s was recorded on 13 December. On the contrary, January 2002 was characterized by relatively stable weather conditions with very few episodes of strong winds, which did not exceed 15 m/s as a mean hourly value. In May 2002, the weather conditions were characterized by highly variable winds both in direction and intensity. The maximum hourly speed did not exceed 11 m/s. June 2002 was characterized by variable wind conditions, but southeasterly winds prevailed most of the time. Their maximum hourly speed of about 14 m/s was recorded on 5 June, when 'acqua alta' phenomenon occurred in Venice (Gačić et al., 2004). Relatively low winds of variable direction persisted in the middle of the month. Only the last week in June was under the influence of a strong NE bora wind, with a maximum mean hourly speed of about 16 m/s, interrupted shortly with moderate SE winds.

3.3.3. Case study: NE bora wind

A strong bora event occurred in the first half of December 2001. A sequence of snapshots presenting subtidal current maps every 36 h between 6 December, 18:00, and 11 December, 06:00, is given in Fig. 10, showing an evolution of the current field during this wind episode. Maximum mean hourly wind speed observed within this period was about 20 m/s.

The first map in the sequence (Fig. 10a) refers still to a low and variable wind. The current field is not uniform, and near the Lido Island, a small anticyclonic eddy of about 4 km in diameter can be observed. Speeds are less than 10 cm/s. Due to the incomplete spatial coverage to the south of the Malamocco inlet, we have only a hint of the presence of a similar eddy there. Along the outer border of this small-scale feature, there is a southward, southwestward flow, which gradually decreases offshore from about 15 cm/s to less than 10 cm/s. The next snapshot (Fig. 10b) shows already well-developed bora wind (about 14 m/s). The current field becomes more uniform over the region, having prevalently southwestward direction with speeds of about 10 cm/s. As the wind persists and increases in speed (Fig. 10c), a strong coastal current develops, reaching a maximum of 30 cm/s in an approximately 3-km wide coastal strip. Small-scale features, such as the earlier observed clockwise eddies, disappear. The strong coastal flow is a consequence of the geostrophic adjustment to the increased horizontal pressure gradient between nearshore and offshore regions due to the wind setup. The last map of the sequence (Fig. 10d) showing a low northerly wind refers to the end of this bora episode. The current field is much more uniform in intensity (about 20 cm/s) over most of the region, there is no more strong coastal flow, and the flow is decreasing in the vicinity of the shore. During another strong bora episode occurring shortly after, with a maximum hourly speed of 23 m/s observed on 13 December, the time evolution of the surface flow was similar. However, the maximum southward flow, which was quite uniform over the study area, reached 50 cm/s.

3.3.4. Case study: SE sirocco wind

We are particularly concerned with the episode of the sirocco (SE wind) in June 2002, characterized also by the 'acqua alta' phenomenon. The evolution of the flow is represented through a sequence of six snapshots taken every 12 h in the interval between 5 June, 00:00 UTC, and 7 June, 12:00 UTC (Fig. 11).

The first map (Fig. 11a) is characterized by a low southeasterly wind (4 m/s). The flow is quite nonuniform, and a strong horizontal shear between the onshore and offshore area is evident. At the outermost zone, southward flow is weak, while near the shore, north or northwestward flow is observed. The anticyclonic curvature of the currents to the north may be an indication of the presence of an eddy. The subsequent map (Fig. 11b) shows an increase of the wind speed up to about 9 m/s. The current flow in a major portion of the study area assumes the downwind direction, with velocities up to 20 cm/s. Twelve hours later (Fig. 11c), the wind speed increases and reaches 10 m/s. The flow in the northern portion is still toward the coast inducing, as during the bora

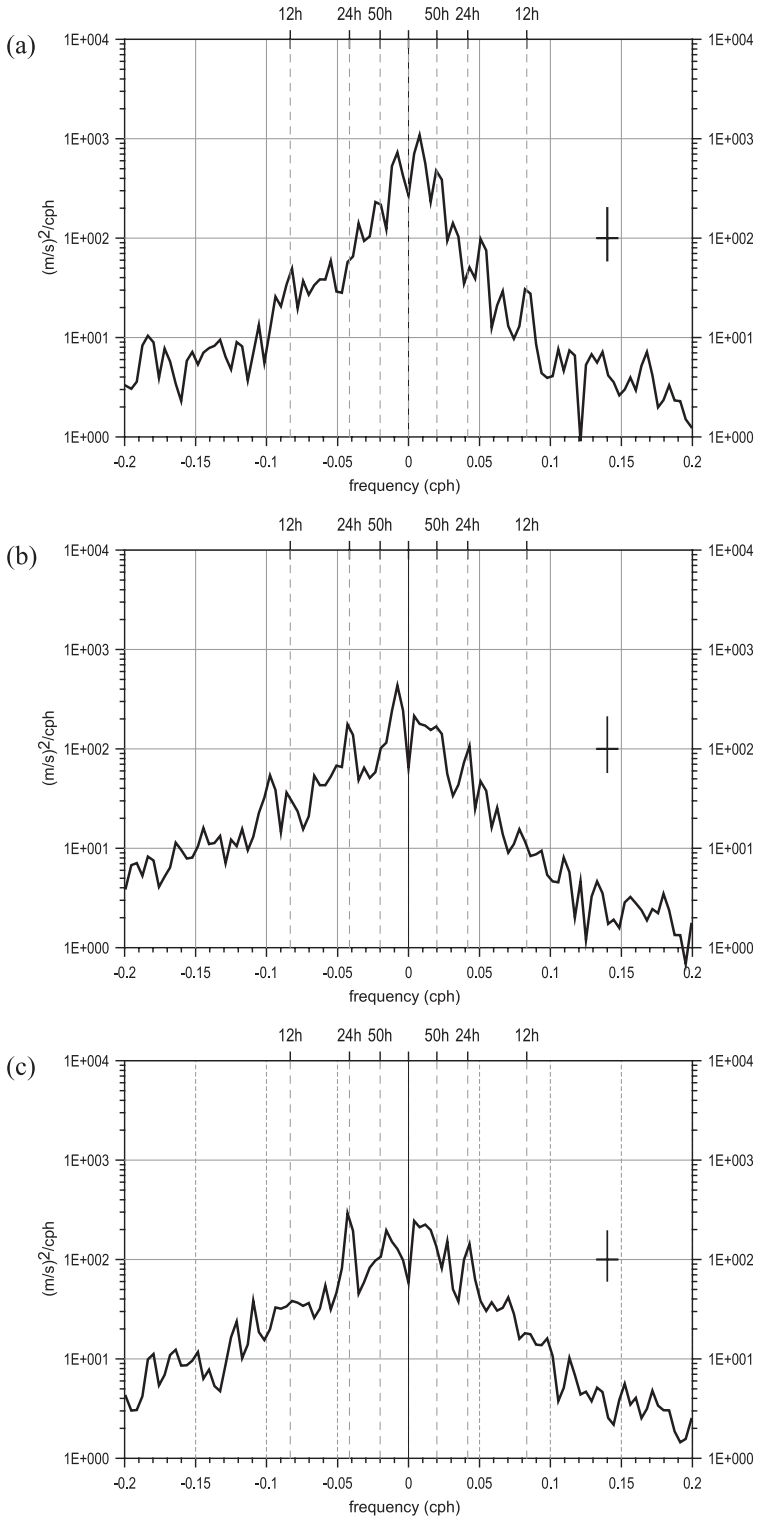
(a)
(b)
(c)
12h
24h
50h
50h
24h
12h
1E+004
1E+003
1E+002
1E+001
1E+000
(m/s)2/cph
-0.2
-0.15
-0.1
-0.05
0
0.05
0.1
0.15
0.2
frequency (cph)

episode, a wind set up near the land and a consequent increase of the cross-shore pressure gradient. A subsequent geostrophic adjustment leads to a formation of the southward flow whose core is detached from the coast, and at some 5 km away, reaches a maximum of 20 cm/s, decreasing both in the onshore and offshore directions (Fig. 11d). As the wind changes (Fig. 11e), the flow reveals a more complex structure characterized by a weak anticyclonic eddy between the inlets of Lido and Malamocco, by a relatively strong southeastward flow (more than 20 cm/s) in the central zone and by a horizontal shear in both the shoreward and seaward directions. Finally, the southwesterly wind ceases (Fig. 11f), while the flow exhibits a strong shear between the northward coastal flow and southward flow offshore. The structure of the current vectors indicates again the possible presence of two clockwise eddies situated northeastward and southeastward of the Malamocco inlet.

3.3.5. Case study: variable and low wind

This example refers to variable wind conditions during the time interval between May 8 and May 15, 2002 (Fig. 9). A sequence of maps taken every 24 hours starting from May 8, 06:00, is presented in Fig. 12. Weak east–northeasterly wind (4–8 m/s) represents local wind conditions at that time. The initial current flow of about 20 cm/s in the southwestward direction (Fig. 12a) gradually rotated clockwise with the wind and assumed an onshore direction (the whole sequence is not presented here). When the wind direction turned to be east–northeasterly, the current field assumed a prevalent northwestward direction (Fig. 12b). On the following day (Fig. 12c), under a weak wind, the current field becomes quite nonuniform with two eddies rotating clockwise near to shore and eastward flow further offshore. Subsequently (Fig. 12d), the two-eddy system turns into a kind of dipole, with counterclockwise rotation to the left and clockwise rotation to the right with respect to the northeastward jet from the Malamocco inlet. Current intensity within the eddies reaches at most 10–15 cm/s. A day later (Fig. 12e), the dipole starts to transform, maintaining its southern branch. Currents are stronger at the eastern margin of the study area. In Fig. 12f–h, while the wind is still weak, almost the whole area is under the influence of the north, northeastward flow, which tends to turn southward in the easternmost portion of the study area. Such a persistent current reversal cannot be attributed to local wind conditions. Due to the limited area of observations, we are not able to delimit the spatial dimensions of this counterflow, neither can we adequately explain its existence. Complex and varying patterns depicted by this sequence of maps testify to the occasional formation of small-scale structures and reversals, which, in the absence of wind, may persist for a couple of days.

3.4. Mean annual and monthly surface flow

Maps of the mean current field at yearly and monthly time scales were constructed from the nontidal time series on a subsampled grid. For the sake of legibility, these maps omit every other grid point along diagonal lines running through the study area. In addition, only those grid points having not more than 30% of the data missing were used. Due to this constraint, the study area was not uniformly covered. For example, coverage for the months of March and June was noticeably reduced. Monthly mean current maps and the corresponding [EKE] are presented below for the entire year of investigation.

The mean surface currents calculated for the 1 year of measurements are plotted in Fig. 13. They show that the long-term mean flow is oriented southward. The maximum velocities (12 cm/s) are contained within a 5-km wide central zone. The speed slightly diminishes (<10 cm/s) toward the open sea. Horizontal shear is stronger on the coastal side of the stream, where currents drop to less than 5 cm/s near the shore. The orientation and speeds are modified in the vicinity of the Malamocco inlet, influenced probably by the morphology of the inlet jetties, as anticipated already by Gatto (1984).

Fig. 8. Two-sided rotary spectrum of hourly winds from the Oceanographic Platform (see Fig. 1 for the anemometer location). Three different time intervals approximately correspond to those of the current: AW (a), Sp (b), and Su (c). Vertical and horizontal error bars denote the 95% confidence level and a frequency resolution, respectively. Negative frequencies refer to the clockwise (anticyclonic) motions, while positive frequencies refer to the counterclockwise (cyclonic) motions. The area below the curve corresponds to the total variance.

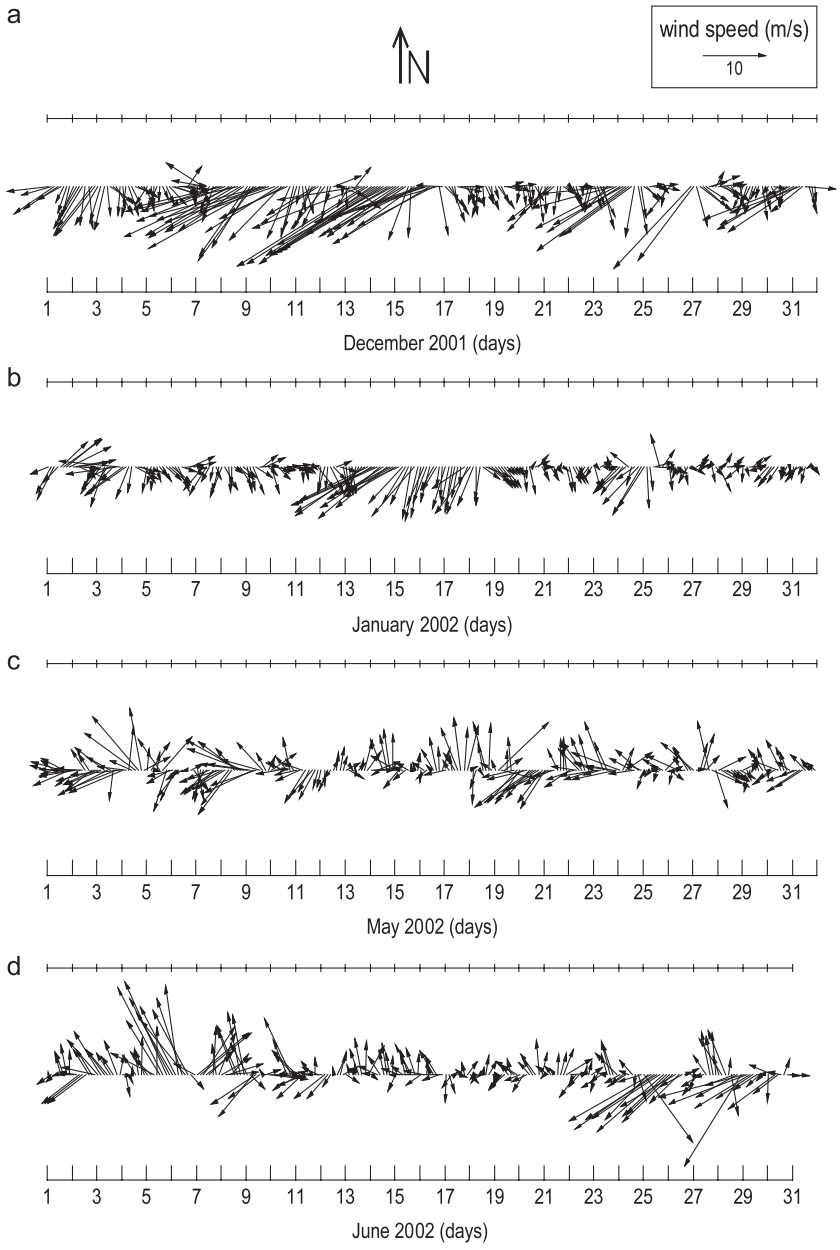

Fig. 9. Mean hourly winds from the Oceanographic Platform as measured during December 2001 (a), January 2002 (b), May 2002 (c), and June 2002 (d). Wind vectors are plotted every 3 h for the sake of legibility.

The monthly sequence of currents in Fig. 14 shows that some characteristics of the yearly mean flow remain invariant throughout the various seasons. This regards especially the orientation of the flow, which remains southward throughout the year. In November and December 2001, monthly mean maps reveal relatively intensified flow in the central area, with respect to open sea. Maximum value for the speed is 16 and 17 cm/s in November and December, respectively. The current diminishes in a very narrow coastal strip. In January 2002, the mean flow is weaker (maximum monthly flow is about 12

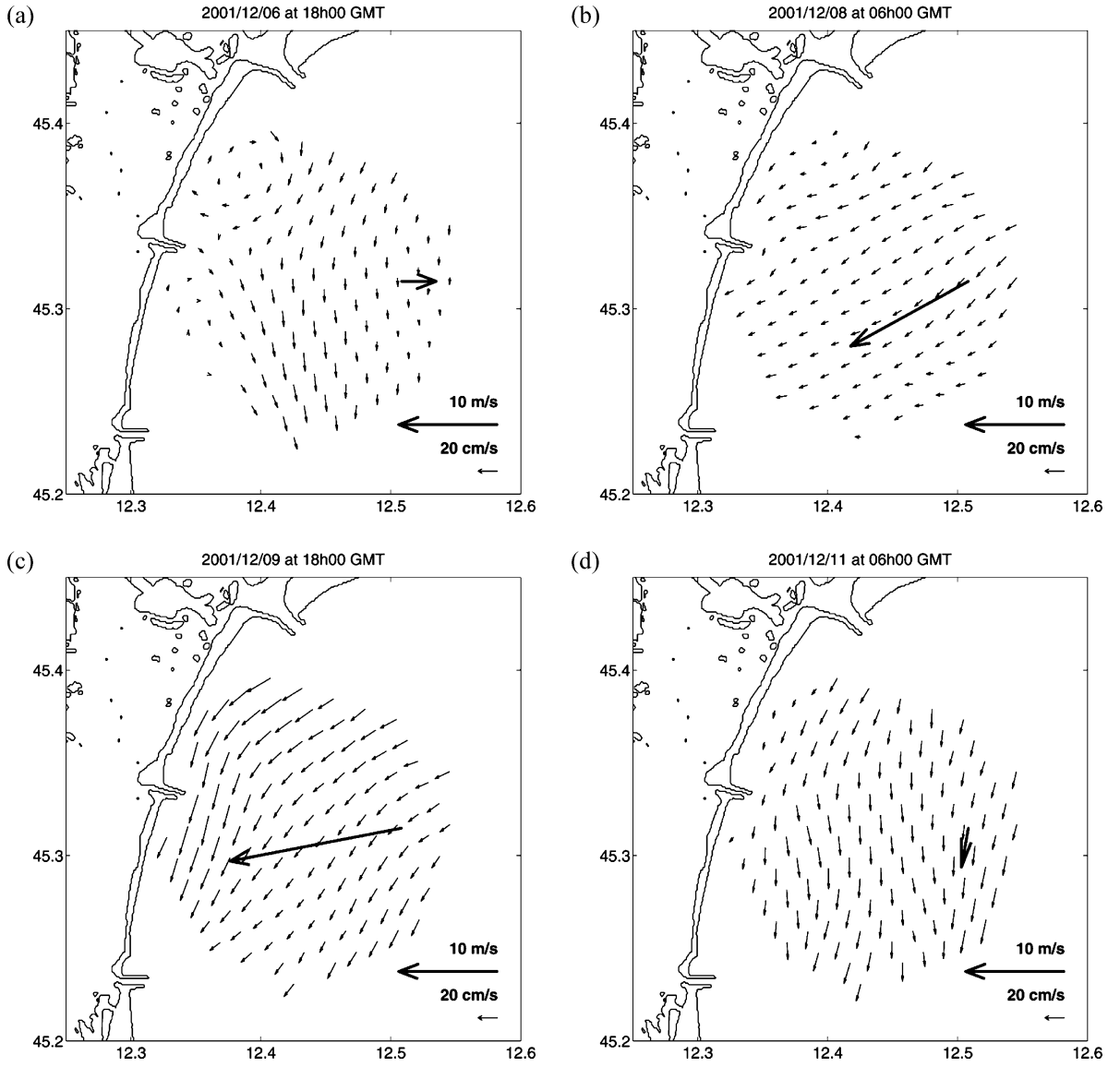

Fig. 10. Sequence of the hourly vector maps of current (thin line) and wind (thick line) during an episode of the strong NE bora wind reported every 36 h between December 6, 18 h, and December 11, 06 h, 2001. Current vectors refer to the subtidal currents.

cm/s) and the horizontal shear between the eastern and western portions of the study zone is smaller. In February and March 2002, the flow is a bit more intense (up to 13 cm/s). In April 2002, there is again a horizontal shear evident between the open sea and the zone about 4 km distant from the coast. There, the flow reaches a maximum of 16 cm/s, while to the east, it is about 6 cm/s. In May 2002, the mean residual flow reaches a minimum for the whole period of investigation. The largest speed is 10 cm/s. In addition, the spatial pattern has changed, becoming rather nonuniform and revealing the presence of small-scale structures: shear between the NW zone and the rest of the area is evident, while just south of the Malamocco inlet, an anticyclonic eddy of about 3 km in diameter can be seen. Anticyclonic curvature of the flow to the north might indicate the frequent presence of another eddy. The flow diminishes

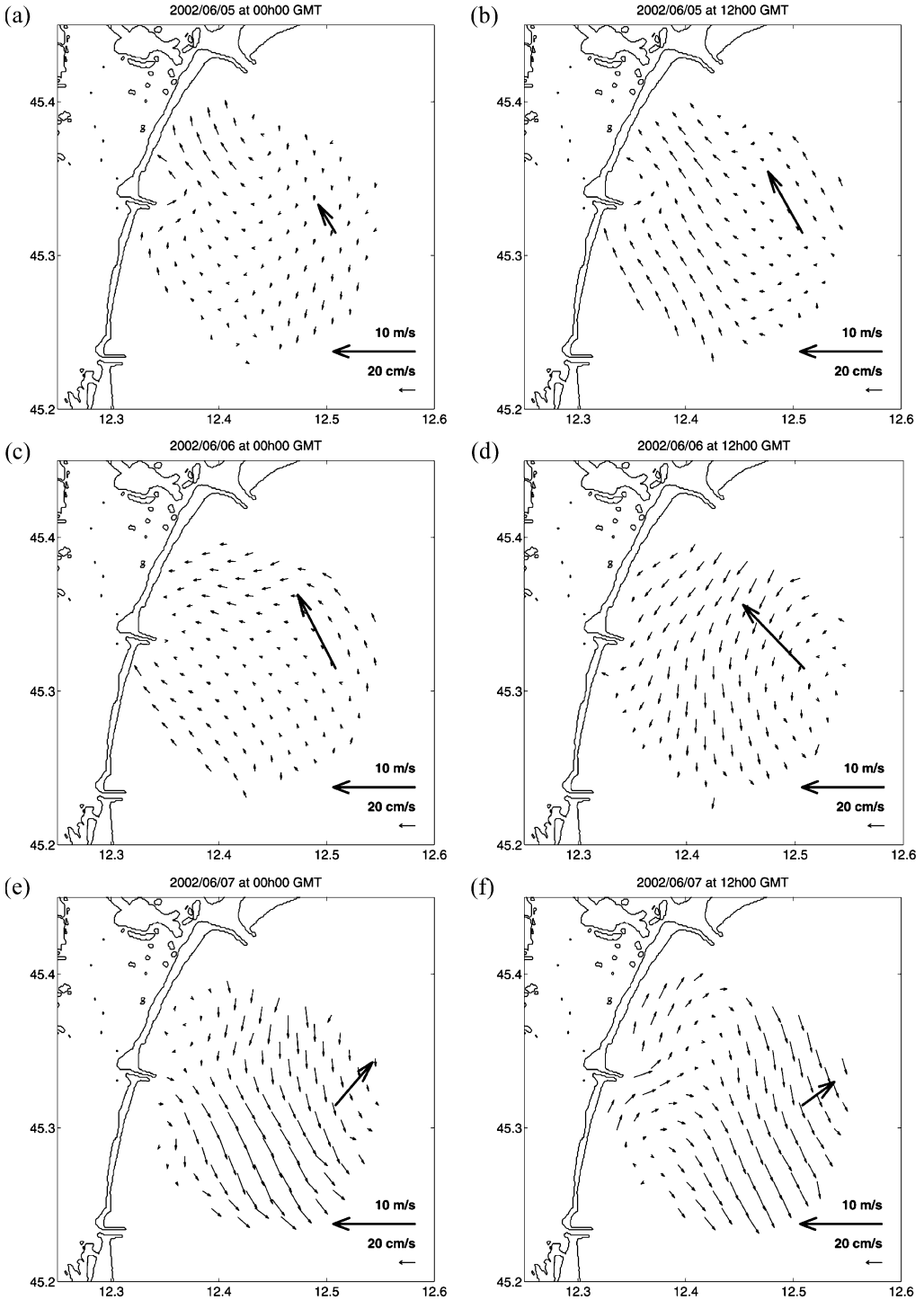

Fig. 11. Sequence of the hourly vector maps of current (thin line) and wind (thick line) during an episode of SE sirocco wind concomitant with the 'acqua alta' event in Venice, taken every 12 h in the interval between 5 June, 00 h, and June 7, 12 h, 2002. Current vectors refer to the subtidal currents.

offshore. In June 2002, flow near the inlet is weak, while in the open sea, it is reinforced and reaches a maximum value of 14 cm/s. In July 2002, the intensity distribution is relatively homogenous, showing a decrease only near the coast and hinting again at the presence of an anticyclonic eddy to the south of the Malamocco inlet. Maximum speeds are about 15 cm/s. In August 2002, almost the same characteristics can be observed, except that the flow intensity is diminished to about 11 cm/s. In September and October 2002, the flow becomes similar to that observed in early spring when the jet is detached from the coast. Maximum speeds are 17 and 16 cm/s in September and October, respectively.

Hence, a common feature of the monthly flow fields is the presence of a southward flow, which during some months is confined near the shore (e.g., November, December, January, February, April, September, and October) and in other months is detached from the shore (e.g., June and July). Near the Malamocco inlet, the mean flow is disturbed. Moreover, north and south of the inlet, small-scale eddies of about 3–4 km in diameter reveal probably the influence of the morphological obstacles induced by the jetties built at the inlets. This is especially evident when wind forcing is weak as in May, July, and August.

3.5. Eddy kinetic energy maps

One of the properties that indicates variability of the flow around the mean is [EKE], which is related to the flow variance. The actual [EKE] described here, obtained from the nontidal currents, contains variations around the monthly mean from fluctuations having subtidal and inertial frequencies (Fig. 7). A monthly sequence of [EKE], associated with the mean monthly current fields from Fig. 14, is reported in Fig. 15. Throughout the autumn and winter months, the maximum [EKE] is limited either to the vicinity of the central inlet, and to marginal areas toward the other two inlets (e.g., November 2001), or in general to the entire coastal strip (e.g., December 2001). In the central zone, [EKE] values are mostly smaller. This type of a spatial structure indicates more significant current variability in the coastal region than at the open sea, and it might be explained by a low-frequency variability induced by the wind. Exceptionally, in January 2002, almost the entire study area is characterized by relatively low variability. As already mentioned, this might be a result of stable meteorological conditions during this month characterized by weak wind activity (Fig. 8) and low freshwater input into the Northern Adriatic due to a small Po River discharge rate (not shown here). From May to August 2002, the spatial properties of the variability change and the values of [EKE] in the eastern portion of the study area toward the open sea become equal or even greater than those in the coastal area. The reason for this is a decrease of the low-frequency variability compared with that induced by winter meteorological conditions and an increase of the inertial variability, which during late spring and summer, when the water column is stratified, develops in the offshore areas. In October 2002, the variability again becomes stronger in the near-shore area. A peculiar situation is evident in the month of May when the maximum [EKE] is associated with the mean monthly flow the entire observation period.

For comparison with the HF radar-derived surface currents, values of [EKE] computed for the along-channel, nontidal flow of the near-surface cells from ADCPs moored in the lagoon inlets are reported for each month. This nontidal flow within the inlet contains mostly free oscillations (seiches) and some portion of the low-frequency motions due to the wind (Gačić et al., 2004). In some cases, [EKE] smoothly varies approaching the Malamocco inlet like in December 2001, January 2002, and July 2002 (Fig. 15), but sometimes the transition is not so gradual, as for instance in November 2001, February 2002, or March 2002 (Fig. 15). This illustrates that currents in the inlet respond differently than do offshore surface currents to the same possible forcing mechanisms acting over local and regional spatial scales.

We are aware that some of the patterns in the [EKE] maps deserve more detailed and cautious interpretation. Namely, some of the patterns connected to the maximum values are at the margins of the study area, which are considered less reliable than the central zone due to lower data returns and poorer geometric combinations of the radial currents used to create the vector surface current maps. In addition, errors grow quickly for nonlinear quantities, such as [EKE]. The monthly mean flows for the area depicted

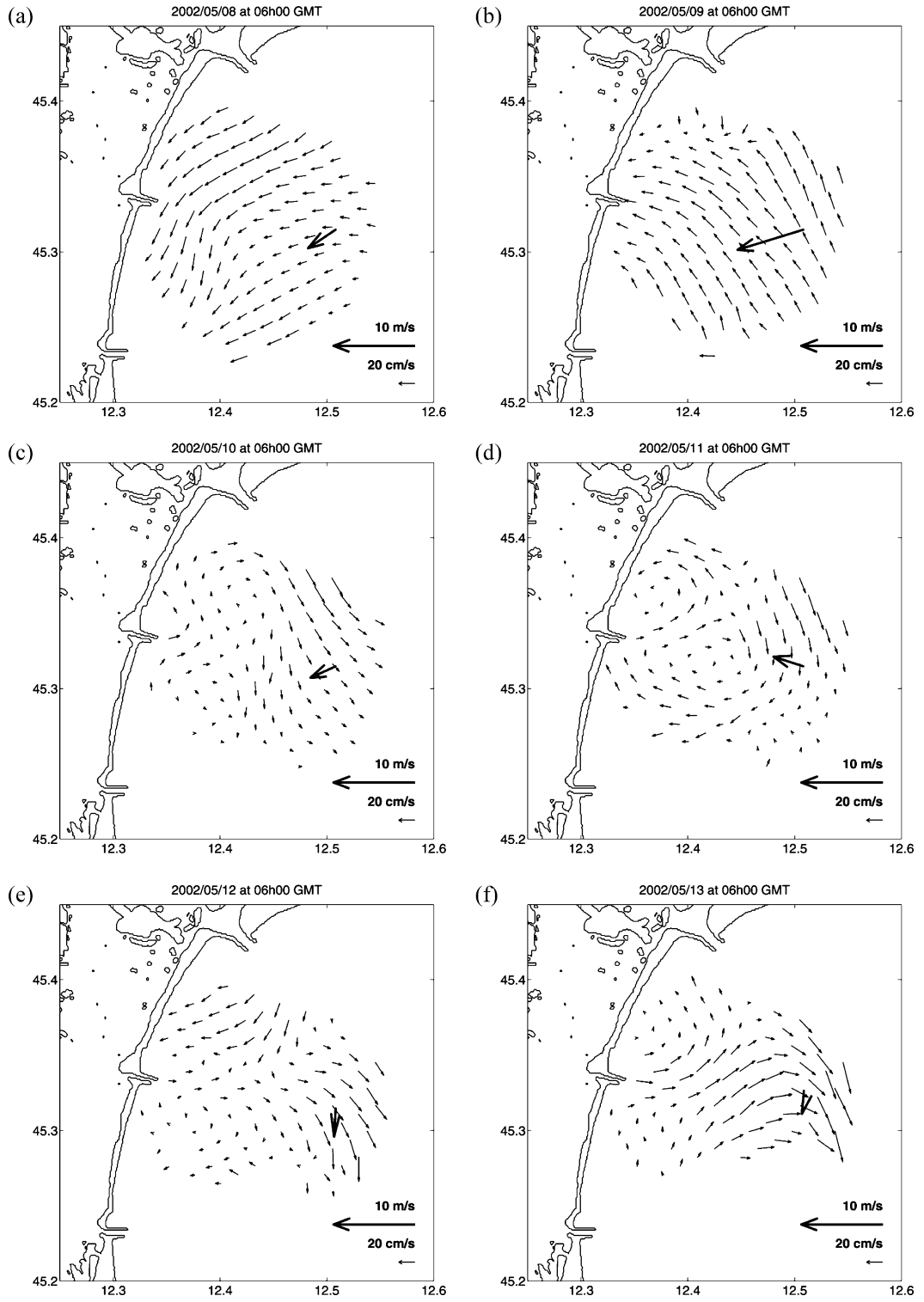
(a)
2002/05/08 at 06h00 GMT
(b)
2002/05/09 at 06h00 GMT
(c)
2002/05/10 at 06h00 GMT
(d)
2002/05/11 at 06h00 GMT
(e)
2002/05/12 at 06h00 GMT
(f)
2002/05/13 at 06h00 GMT
10 m/s
20 cm/s
45.4
45.3
45.2
12.3
12.4
12.5
12.6

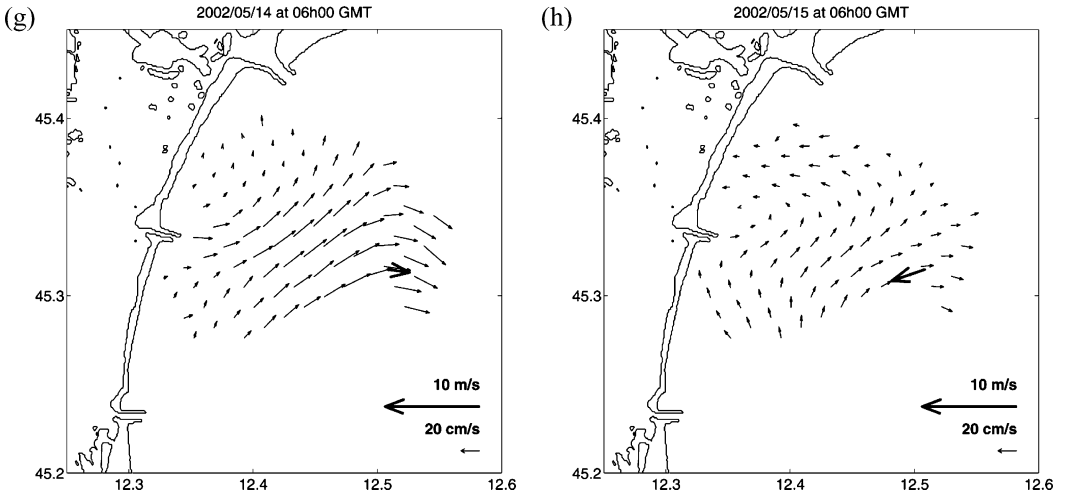

Fig. 12. Sequence of hourly vector maps of current (thin line) in cm/s and wind (thick line) in m/s during variable winds, taken every 24 hours between 8 May, 06 h and 15 May, 06 h, 2002. Current vectors refer to the subtidal currents.

in Fig. 2 do not show any incoherent patterns at the margins of the region. Therefore, we have decided to maintain the same area for the presentation of [EKE], although some of the variabilities connected to the [EKE] patterns may be suspicious. On the other hand, this is the first observational evidence on the surface current variability over the zone, and some phenomena may be realistic although observed for the first time from the experimental data. Some indirectly derived characteristics of the circulation in this area (Gatto, 1984) point to mesoscale features as the source of surface flow variability in the region. Moreover, a preliminary analysis of the subtidal currents indicates the presence of small-scale vortices in front of the islands of Lido and Pelestrina (Paduan et al., 2003) that seem to develop as a result of the morphological influence of the jetties in absence of the winds, just like an example given in Section 3.4. Such structures may contribute significantly to the [EKE] increase observed in May 2002. Finally, with regard to model representations of current variability in the region, we note that although the domain of the numerical models is capable now of resolving small-scale structures, recent modelling efforts deal predominantly with the case studies, like in Cucco and Umgiesser (2002), and do not show all the possible aspects of the circulation in front of the Venetian Lagoon.

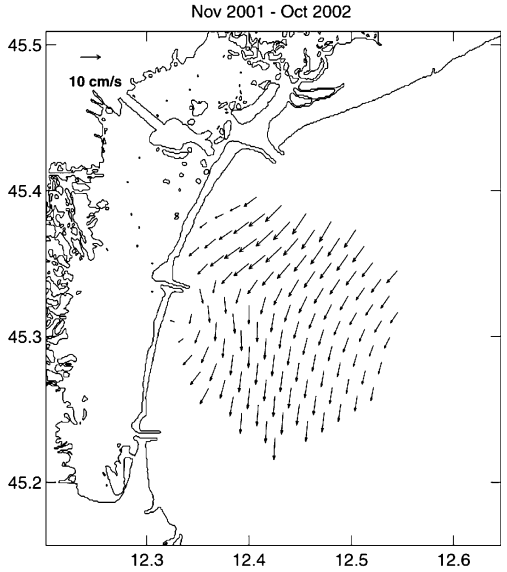

Fig. 13. Mean annual flow pattern in front of the Venetian Lagoon, based on the detided (nontidal) hourly currents.

4. Discussion and conclusions

In this paper, we reported on some of the main circulation properties derived from a 1-year-long time series of hourly surface currents. The results derive from a network of HF radar systems situated in front

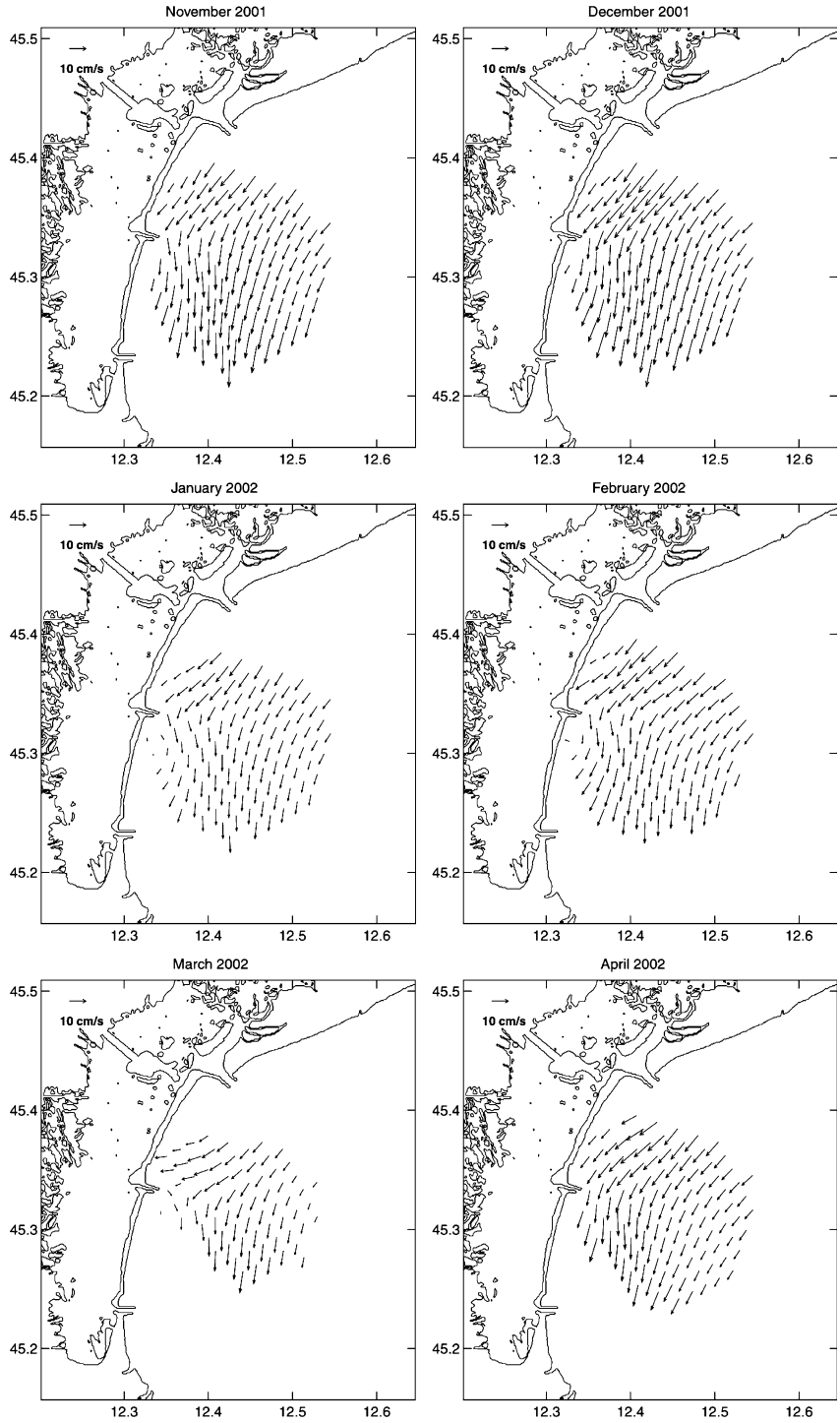

Fig. 14. Sequence of mean monthly flow patterns in front of the Venetian Lagoon, based on the detided (nontidal) hourly currents for the time interval November 2001–October 2002.

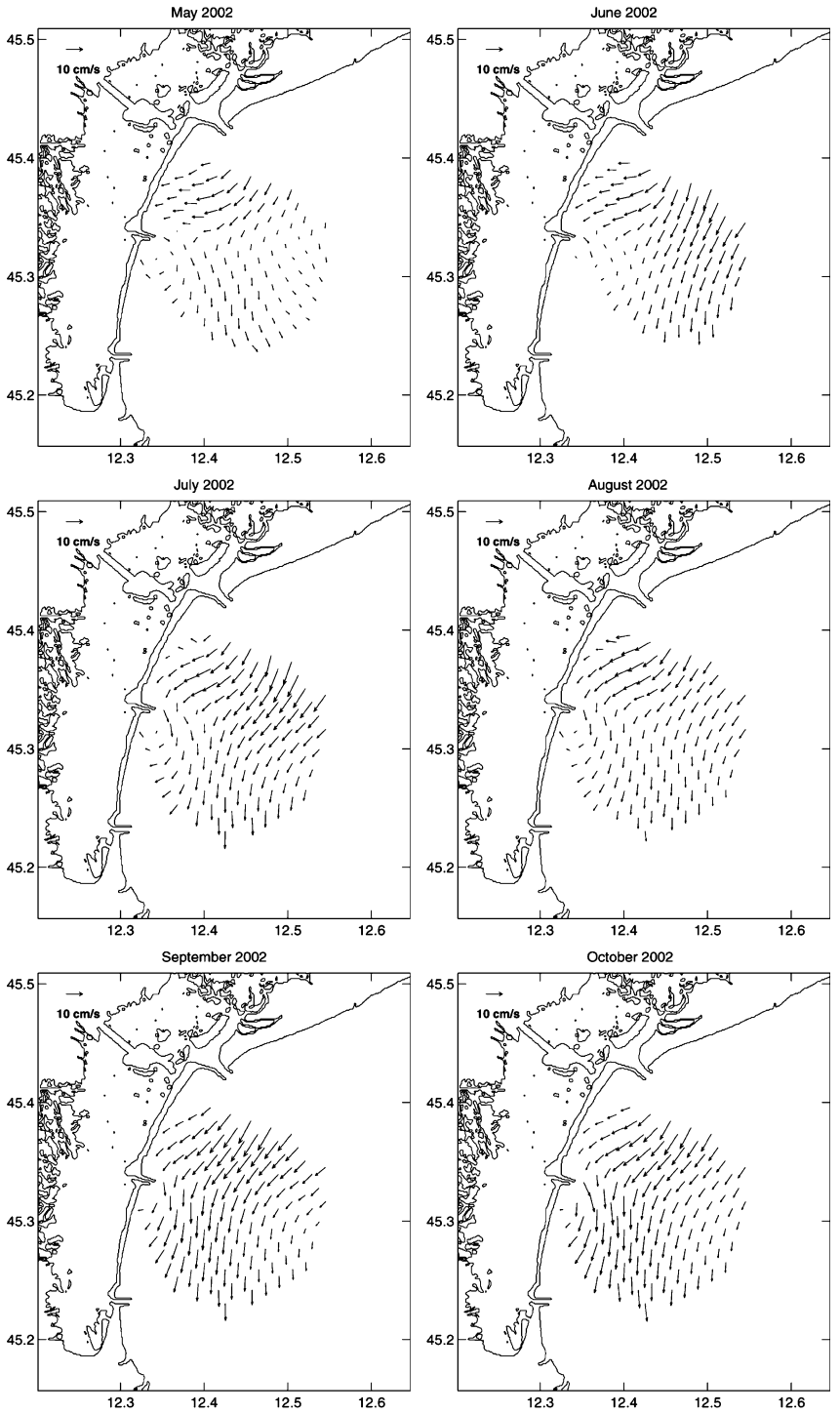

Fig. 14 (*continued*).

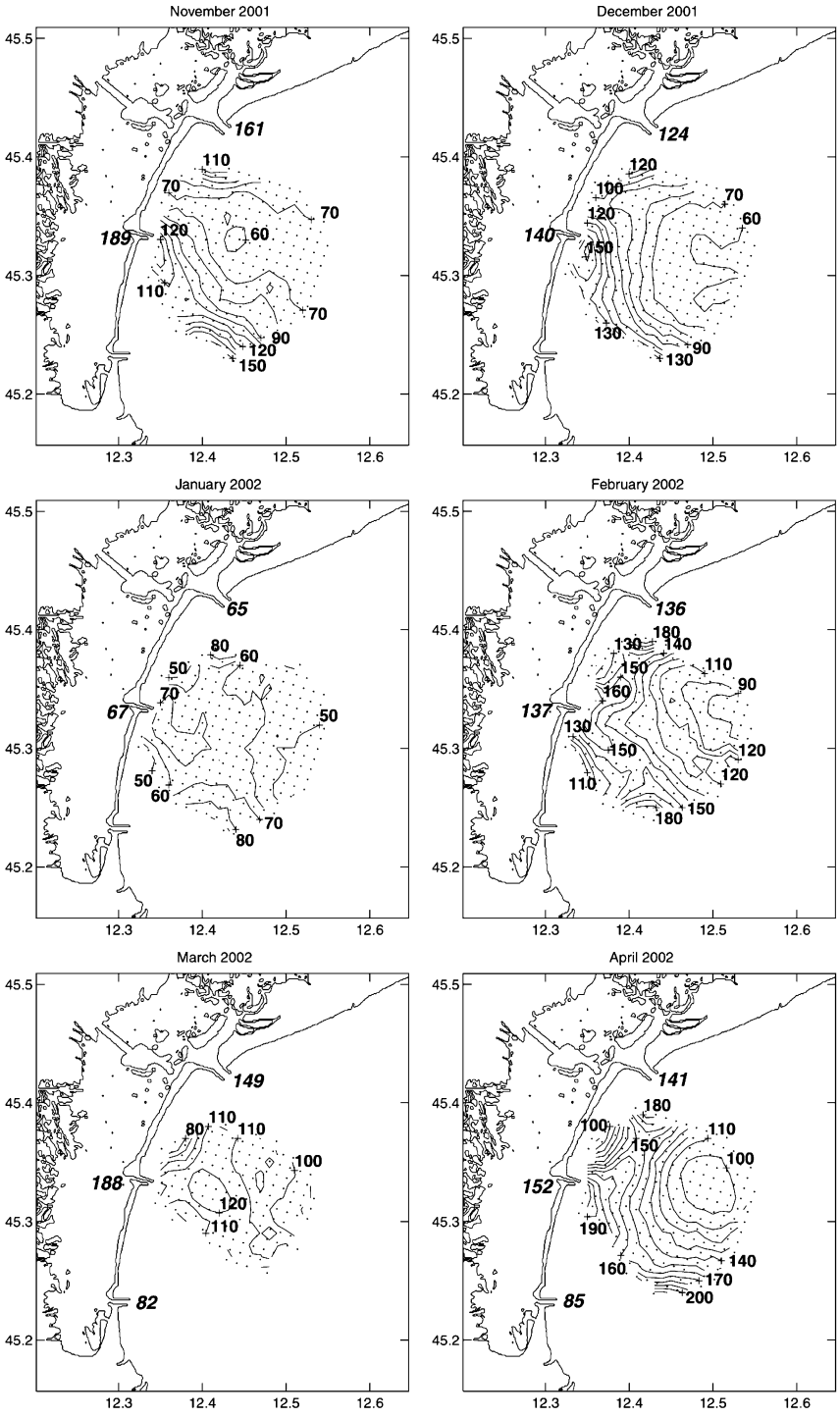

Fig. 15. Sequence of maps representing a mean monthly eddy kinetic energy per unit mass (cm^2/s^2) for the time interval November 2001–October 2002.

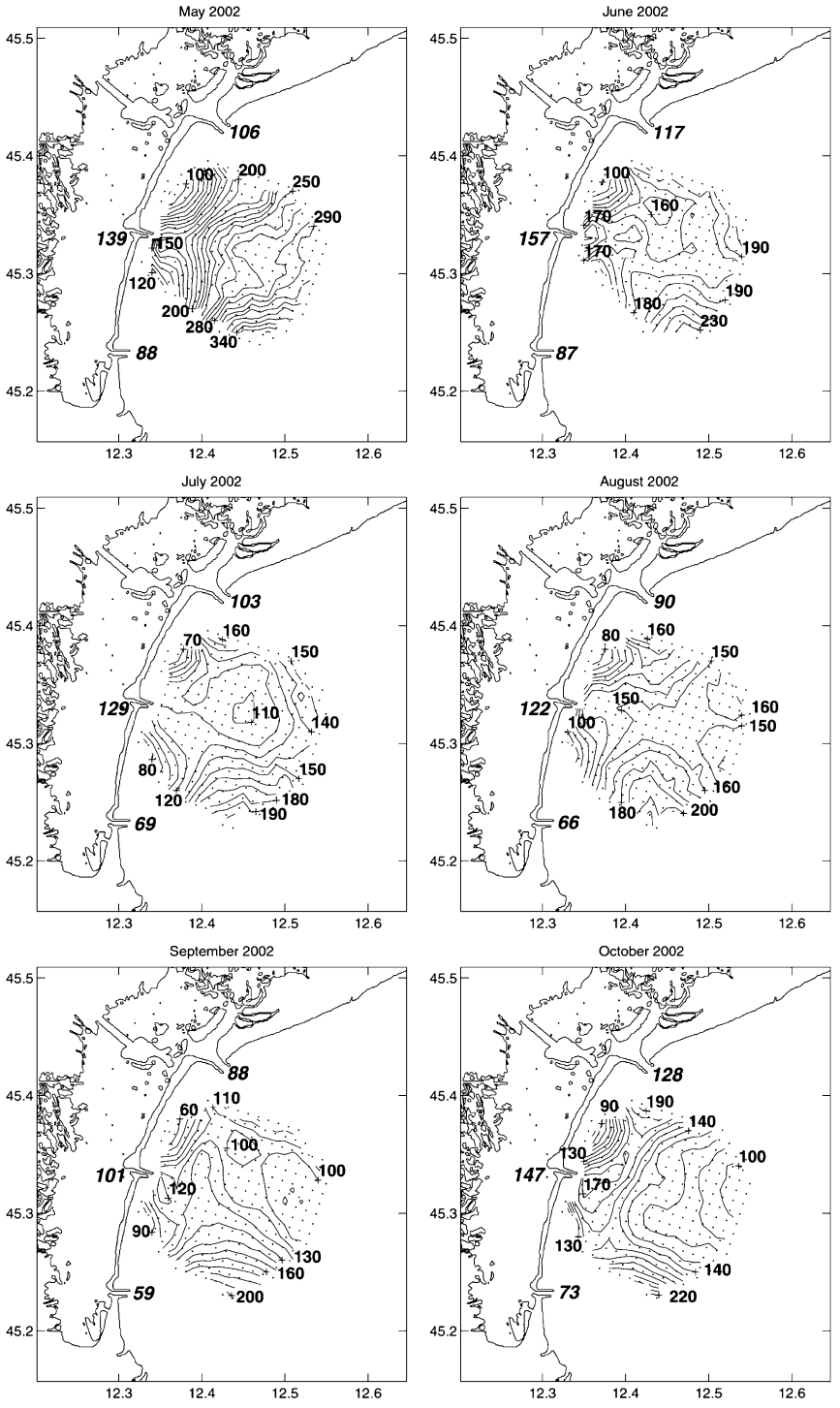

Fig. 15 (*continued*).

of the Venetian Lagoon. Although the HF radar measurements are restricted to the very surface layer (upper 1 m), they provide extensive experimental evidence of prominent aspects of the local circulation. A primary description of the flow in this area is the net flow, which is of the order of 10 cm/s, oriented southward. This result is in conformity with the well-known surface cyclonic cell of the general circulation in the Adriatic Sea and the subbasin circulation within its northernmost portion. This historical view of the Adriatic Sea circulation has been derived from numerous observations, both direct and indirect (e.g., drifters; thermohaline properties), as reviewed by Poulain and Cushman-Roisin (2001).

In addition to observations of the mean currents, HF radar measurements provide evidence about current variability both in time and space. Temporal scales range from tidal and inertial to subtidal. The circular-shaped area covered by the measurements, with a surface area of about 120 km^2 and a spatial resolution of about 750 m, enables detection of the variability from mesoscale to subbasin scales. Unlike within the lagoon inlets, where the flow is almost entirely due to the tidal motion, the relative contribution of tides to the flow variability decreases from 20% near the inlets to 10% at the offshore limits of the study area. Most of the amplitudes of the seven commonly analysed constituents are one order of magnitude smaller than in the inlets (Gačić et al., 2004) and reach only a few cm/s. Moreover, the structure of the tidal signal changes: near the inlet, semidiurnal M2 oscillations prevail while diurnal K1 fluctuations dominate at the open sea boundaries. In addition, long-term constituents (time scales ranging from 2 weeks to 6 months) appear more important than some diurnal and semidiurnal constituents. The spatial distribution of the tidal phases, at least for the most significant diurnal (K1) and semidiurnal (M2) constituents, is distorted in the vicinity of the inlet. Semimajor axes of the tidal ellipses reach maximum values of 6–7 cm/s for the M2 constituent in the vicinity of the inlet. Tidal energy dissipates rapidly and already 4–5 km offshore the semimajor axis is typically 2–4 cm/s. These results are consistent with those derived from experimental and modelling studies of the tidal motions in the Northern Adriatic as reviewed by Cushman-Roisin et al. (2001), although none of the existing studies focused with great detail on our study area.

The detided (or nontidal) currents are to a large extent influenced by the variability at synoptic time scales (low-frequency band) during winter near the coast. During the warm season, the region of maximum variability shifts toward the open sea, where inertial motions contribute significantly to the current variability. The local variance maximum at the diurnal band can be explained in terms of the combined influence of the seiche activity and sea breeze forcing.

During low-wind or calm weather conditions, the structure of the flow assumes a different pattern: in the vicinity of the islands of Lido and Pelestina, mostly clockwise eddies of about 4–5 km in diameter may form, as illustrated by an example from May 2002. These eddies can persist for some time and remain evident even on a monthly time scale, like in May and July. Speeds are relatively low (about 5 cm/s). However, these local phenomena may contribute significantly to the eddy kinetic energy increase observed near the coast.

Two wind conditions are characteristic for the Northern Adriatic: northeasterly (bora) and southeasterly (sirocco) winds. Both are associated with meteorological disturbances passing over the region (see Poulain and Raicich, 2001 for a review). The time period between November 2001 and October 2002, however, was somewhat anomalous in that sirocco winds were almost absent during autumn and winter. One of the strongest bora events throughout the study period, that in mid-December 2001, was chosen to illustrate how the current field adjusts to such a wind forcing. Intensification of the near coastal southward current, homogenisation of the current flow, and decreased horizontal shear between the coastal strip and open sea are the most relevant characteristics of such an event. Current speeds may reach 50 cm/s. In contrast, the sirocco wind may induce a temporary current reversal from the dominant southward to a northward direction, as during the event at the beginning of June 2002. This has been observed and corroborated by numerical models like that by Orlić et al. (1994) and evidenced using the same HF radar technique in other coastal regions along the western coast of the Adriatic (Kovačević et al., 2000). In the June 2002 event, the transient reversal ceases giving way again to a southward coastal flow, while the onset of inertial motions is observed offshore.

As far as the possible range of low-frequency forcing is concerned, in this paper, we addressed exclusively the wind, and in particular, the local wind. As summarized by Poulain and Cushman-Roisin (2001), winds are the drivers for most of the transient currents in the Adriatic Sea. The effects of stratification during the warm season—in contrast to the vertically homogeneous water column during a cold season—are observed indirectly through the increased occurrence of inertial oscillations.

Intra-annual variability of the current field was illustrated by a sequence of mean monthly current maps for the period of investigation from November 2001 to October 2002. The mean monthly flow is always southward. Just in the vicinity of the Malamocco inlet, it becomes susceptible to the influence of the inlet jetties. From month to month, the speed fluctuates, reaching maximum values between 9 and 18 cm/s. The most intense flow is observed during the autumn months in November–December 2001 and September–October 2002. The minimum flow during the cold season is observed in January 2002, possibly due to weak forcing (low meteorological activity and consequent low freshwater discharge into the Northern Adriatic). Weak flow is also observed during May 2002.

The spatial resolution of the HF radar measurements described here does not allow for the resolution of the characteristics of the flow in regions very close to the inlets. However, it does provide evidence that the influence of flow in the inlets, driven mainly by tidal and other high-frequency motions like the 22- and 11-h Adriatic seiches, rapidly decreases within a plume of a 3–4 km diameter. The effect of the seiches, which contain a significant portion of the variance within the inlets (Gačić et al., 2004), is not detectable in the HF radar-derived surface currents, possibly because they also decrease rapidly away from the inlets.

The spatial resolution of the HF radar-derived currents is sufficient to detect recurrent small-scale features, such as the frequently seen clockwise eddies north and south of the Malamocco inlet. Those features are 4–5 km in diameter and are most commonly observed during low wind events. In this data set, these features are most common in May and July when they are even detectable in the monthly averaged maps. At the same time, the strongest variability on a monthly scale occurs during May, associated to a certain extent with variable wind conditions and the onset of inertial oscillations near the open sea boundary, as well as to the evolution of the small-scale eddies near the inlet.

We maintain that the present study has just opened a new chapter regarding surface flow variability in the near-coastal area in front of the Venetian Lagoon. Our approach has been aimed at: (1) data treatment necessary to obtain correct time series in all the possible grid nodes over the investigated area and (2) description of the principal characteristics of the surface flow and its spatial and temporal variability within a 1-year time interval. Some topics remain for a future work, such as a more detailed study of the relationship between the local and remote wind in some particular situations and a quantification of the current response (e.g., Paduan and Rosenfeld, 1996; Prandle and Ryder, 1989; Prandle, 1987). Future studies could be focused also on performing a comparison with numerical modelling results (e.g., Lipphardt et al., 2000; Paduan and Shulman, 2004). Of particular interest will be to investigate in more detail the eddy phenomena in the vicinity of the inlets (looking at the favourable conditions for their formation and duration) and to study the convergence–divergence zones, which may be relevant from the ecological point of view (e.g., Graber and Limouzy-Paris, 1997) as well as for the transport of sediments along the littoral of the Venetian Lagoon.

Acknowledgements

This study has been performed in the framework of the CORILA Research Programme 2000–2004, Environmental Processes Area, Line 3.5: Quantity and quality of the exchange between lagoon and sea. One of the authors (Isaac Mancero Mosquera) undertook this work with the support of the “ICTP Programme for Training and Research in Italian Laboratories, Trieste, Italy”. We acknowledge Michael Cook, NPS, Monterey, CA, for supplying a number of routines in MatLab for data processing and plotting (http://www.oc.nps.navy.mil), as well as R. Pawlowicz, R. Beardsley, and S. Lentz for a Tidal Analysis Package in MatLab (ftp://sea-mat.whoi.edu./index.html) derived on the basis of Michael Foreman’s IOS Tidal

package. The wind data from the CNR-Oceanographic Platform 'Acqua Alta' are obtained by the courtesy of Municipality of Venice. Constructive comments and suggestions of the two anonymous reviewers are highly appreciated. The authors are indebted to Jeffrey D. Paduan, NPS, Monterey, CA, for helpful comments on the manuscript, which substantially improved the overall comprehension of the text.

References

Barrick, D.E., Headrick, J.M., Bogle, R.W., Crombie, D.D., 1974. Sea backscatter at HF: interpretation and utilization of the echo. Proc. IEEE 62 (6), 673–680.

Barrick, D.E., Evans, M.W., Weber, B.L., 1977. Ocean surface currents mapped by radar. Science 198, 138–144.

Bergamasco, A., Gačić, M., 1996. Baroclinic response of the Adriatic Sea to an episode of bora wind. J. Phys. Oceanogr. 26, 1354–1369.

Crombie, D.D., 1955. Doppler spectrum of sea echo at 13.56 Mc/s. Nature 175, 681–682.

Cucco, A., Umgiesser, G., 2002. Modelling the water exchanges between the Venice Lagoon and the open sea. In: Campostrini, P. (Ed.), Scientific Research and Safeguarding of Venice, Corila Research Program 2001 Results. Istituto Veneto di Scienze, Lettere ed Arti, Venezia, pp. 499–514.

Cushman-Roisin, B., Malačič, V., Gačić, M., 2001. Tides, seiches, and low-frequency oscillations. In: Cushman-Roisin, B., Gačić, M., Poulain, P.-M., Artegiani, A. (Eds.), Physical Oceanography of the Adriatic Sea. Kluwer Academic Publishing, Dordrecht, pp. 217–240. Chap. 7.

Foreman, M.G.G., 1978. Manual for Tidal Currents Analysis and Prediction. Pacific Marine Science Report 78-6. Institute of Ocean Sciences, Patricia Bay, Sidney, British Columbia. (revised edition 1996).

Gačić, M., Mazzoldi, A., Kovačević, V., Mancero Mosquera, I., Cardin, V., Arena, F., Gelsi, G., 2004. Temporal variations from tidal to seasonal scales of water fluxes between the Venetian Lagoon and the open sea. J. Mar. Syst. 51, 33–47 this issue.

Gatto, P., 1984. Il cordone litoraneo della laguna di Venezia e le cause del suo degrado, Vol. IX. Istituto Veneto di Scienze Lettere ed Arti, Rapporti e Studi, Venezia, pp. 163–193.

Graber, H.C., Limouzy-Paris, C.B., 1997. Transport patterns of tropical reef fish larvae by spin-off eddies in the straits of Florida. Oceanography 10 (No.2), 68–71.

Gurgel, K.-W., Essen, H.-H., Kingsley, S.P., 1999. HF radars: physical limitations and recent developments. Coast. Eng. 37, 201–218.

Kovačević, V., Gačić, M., Mazzoldi, A., Dallaporta, G., Gaspari, A., 2000. Sea-surface currents measured by coastal HF radar off-shore Ancona. Boll. Geof., Teor. Appl. 41, 339–355.

Krajcar, V., Orlić, M., 1995. Seasonal variability of inertial oscillations in the Northern Adriatic. Cont. Shelf Res. 15, 1221–1233.

Lipa, B.J., Barrick, D.E., 1983. Least-squares methods for the extraction of surface currents from CODAR crossed-loop data: application at ARSLOE. IEEE J. Oceanic Eng. OE-8, 226–253.

Lipphardt Jr., B.L., Kirwan Jr., A.D., Grosch, C.E., Lewis, J.K., Paduan, J.D., 2000. Blending HF radar and model velocities in Monterey Bay through normal mode analysis. J. Geophys. Res. 105 (C2), 3425–3450.

Orlić, M., 1987. Oscillations of the inertia period on the Adriatic Sea shelf. Cont. Shelf Res. 7, 577–598.

Orlić, M., Penzar, B., Penzar, I., 1988. Adriatic Sea and land breezes: clockwise versus anticlockwise rotation. J. Appl. Meteorol. 27, 675–679.

Orlić, M., Gačić, M., La Violette, P.E., 1992. The currents and circulation of the Adriatic Sea. Oceanol. Acta 15, 109–124.

Orlić, M., Kuzmić, M., Pasarić, M., 1994. Response of the Adriatic Sea to the bora and sirocco forcing. Cont. Shelf Res. 14, 91–116.

Paduan, J.D., Graber, H.C., 1997. Introduction to HF radar, reality and myth. Oceanography 10, 36–39.

Paduan, J.D., Rosenfeld, L.K., 1996. Remotely sensed surface currents in Monterey Bay from shore-based HF radar. CODAR J Geophys. Res. 101 (no. C9), 20669–20686.

Paduan, J.D., Shulman, I., 2004. CODAR data assimilation in the Monterey Bay area. J. Geophys Res. 109, C7, C07509, doi:10.1029/2003JC001949.

Paduan, J.D., Gačić, M., Kovačević, V., Mancero Mosquera, I., Mazzoldi, A., 2003. Vorticity Patterns Offshore of the Venetian Lagoon from HF Radar Observations. Linea 3.5 Quantita e Qualità degli Scambi tra Laguna e mare, WBS1 Misure dei Parametri Fisici, WBS1.2. Misure di Corrente con Radar HF, Quinto Rapporto di Ricerca, OGS, Relazione RELI-34/2003 OGA-24.

Poulain, P.-M., Cushman-Roisin, B., 2001. Circulation. In: Cushman-Roisin, B., Gačić, M., Poulain, P.-M., Artegiani, A. (Eds.), Physical Oceanography of the Adriatic Sea. Kluwer Academic Publishing, Dordrecht, pp. 67–109. Chap. 3.

Poulain, P.-M., Raicich, F., 2001. Forcings. In: Cushman-Roisin, B., Gačić, M., Poulain, P.-M., Artegiani, A. (Eds.), Physical Oceanography of the Adriatic Sea. Kluwer Academic Publishing, Dordrecht, pp. 45–65. Chap. 2.

Prandle, D., 1987. The fine structure of nearshore tidal and residual circulations revealed by H.F. radar surface current measurements. J Phys. Oceanogr. 17, 231–245.

Prandle, D., Ryder, D.K., 1989. Comparison of the observed (HF radar) and modelled nearshore velocities. Cont. Shelf Res. 9, 941–963.

Raicich, F., 1996. On the fresh water balance of the Adriatic Sea. J. Mar. Syst. 9, 305–319.

Ursella, L., Gačić, M., 2001. Use of the acoustic doppler current profiler (ADCP) in the study of the circulation of the Adriatic Sea. Ann. Geophys. 19, 1183–1193.